Exact factorization of the photon–electron–nuclear wavefunction: Formulation and coupled-trajectory dynamics

Eduarda Sangiogo Gil, David Lauvergnat, Federica Agostini

Exact Factorization of the Photon-Electron-Nuclear Wavefunction: Formulation and Coupled-Trajectory Dynamics

Eduarda Sangiogo Gil,[1,2] David Lauvergnat,[1] and Federica Agostini*[1]

[1)] *Université Paris-Saclay, CNRS, Institut de Chimie Physique UMR8000, 91405, Orsay, France*

[2)] *Institute of Theoretical Chemistry, University of Vienna, Währinger Straße 17, 1090 Vienna, Austria*

(*Electronic mail: federica.agostini@universite-paris-saclay.fr)

We employ the exact-factorization formalism to study the coupled dynamics of photons, electrons, and nuclei at the quantum mechanical level, proposing illustrative examples of model situations of nonadiabatic dynamics and spontaneous emission of electron-nuclear systems in the regime of strong light-matter coupling. We make a particular choice of factorization for such a multi-component system, where the full wavefunction is factored as a conditional electronic amplitude and a marginal photon-nuclear amplitude. Then, we apply the coupled-trajectory mixed quantum-classical (CTMQC) algorithm to perform trajectory-based simulations, by treating photonic and nuclear degrees of freedom on equal footing in terms of classical-like trajectories. The analysis of the time-dependent potentials of the theory along with the assessment of the performance of CTMQC allow us to point out some limitations of the current approximations used in CTMQC. On the other hand, comparing CTMQC with other trajectory-based algorithms, namely multi-trajectory Ehrenfest and Tully surface hopping, demonstrates the better quality of CTMQC predictions.

I. INTRODUCTION

The exact factorization of the time-dependent molecular wavefunction[1–4] has seen numerous applications in the domain of excited-state nonadiabatic dynamics based on the developments of novel "tools" of analysis[5–8] and of trajectory-based algorithms for quantum molecular dynamics[9–25]. The exact factorization implies a rewriting of the molecular time-dependent Schrödinger equation as two coupled equations for the evolution of the electronic conditional amplitude and of the nuclear marginal amplitude. In particular, in formal analogy with the Born-Oppenheimer approximation[26] – but clearly beyond this approximation, the nuclear evolution is expressed as a new *effective* time-dependent Schrödinger equation where the effect of the electrons in their ground state as well as in their excited states is encoded in a time-dependent vector potential and in a time-dependent potential energy surface that adapt in time to the nonadiabatic electronic dynamics. These potentials are the tools that have been applied in several occasions to provide an interpretation of dynamics in the presence of conical intersections alternative to the Born-Oppenheimer framework (and the Born-Huang expansion)[6,7,27]. Following the study of these potentials, trajectory-based algorithms have been developed to approximate them within an on-the-fly molecular-dynamics scheme. In this way, electronic-structure information, in terms of energies, gradients and couplings, is used to reconstruct the time-dependent potentials along the nuclear trajectories[9,11,18].

The exact-factorization formalism has been employed in other contexts, even though perhaps not with the same large variety of applications as the electron-nuclear case. Examples are the studies done on purely electronic systems[28–33] and on photon-electronic or photon-electron-nuclear systems[34–38]. In the present work, we focus on this last problem, namely the quantum dynamics of the photon-electron-nuclear wavefunction governed by a time-dependent Schrödinger equation.

Tokatly[35] and Maitra[34] independently introduced already some years ago the photon degrees of freedom in the exact-factorization formalism for applications of quantum electrodynamics in the context of *molecular polaritons*. The field of polaritonic chemistry started to emerge little over a decade ago[39–41] as a way to affect (photo)chemical reactions by creating hybrid light-matter states, i.e., the polaritons, when the strong-coupling regime between the molecular excitations and confined light is achieved in optical and plasmonic cavities[42–61]. In chemical physics and physical chemistry, we have witnessed a large variety of ideas aiming to reformulate in cavities concepts such as the Born-Oppenheimer approximation[62–64], nonadiabatic dynamics[38,59,60,65–79], density functional theory[80–83] and other electronic-structure theories[84,85], and the exact factorization[34,35]. In this respect, Maitra followed up on her preliminary work with various analysis of the dynamics of electronic and of electron-nuclear systems in optical microcavities in the regime of strong light-matter coupling. In particular, these works drew the connection between the exact factorization and the "usual" polaritonic picture as well as introduced the idea of trajectories to approximate either the nuclear or the photonic dynamics[34,36–38,86].

In the present study, we propose an alternative way of applying the exact factorization to the photon-electron-nuclear wavefunction building up on the encouraging developments briefly recalled above. Specifically, we decompose the problem in terms of a conditional electronic amplitude and a marginal photon-nuclear amplitude aiming (i) to study the behavior of the time-dependent potentials that drive the dynamics of the photonic and of the nuclear degrees of freedom, and (ii) to apply the coupled-trajectory mixed quantum-classical (CTMQC) algorithm, originally developed for the exact factorization of the molecular problem. Our approach treats the nuclear and the photonic degrees of freedom "on the same footing" via the marginal amplitude, thus it differs from previous work where the marginal amplitude was either the nuclear or the photonic wavefunction. As mentioned above, the idea of photonic trajectories was already investigated by

other authors, however, it was done either by using the exact time-dependent potential energy surface – accessible only for model test-cases, which are exactly solvable – or by invoking the mean-field treatment within an Ehrenfest-like dynamics[38,77]. Therefore, we find it interesting to perform exploratory case studies of such an alternative decomposition of the photon-electron-nuclear wavefunction and to explore the performance of CTMQC in this situation.

The paper is organized as follows. In Section II, we construct the theory by introducing the fundamental quantities of our formalism and we recall the derivation of the CTMQC algorithm. In Section III, we study two exactly-solvable models consisting of one nuclear mode and two singlet electronic states, S_0 and S_1. In both cases, the model systems are coupled to a single-mode cavity in resonance with a particular electronic excitation of the system: in model A of Section III B, mimicking the de-excitation process of the nuclear wavepacket via an avoided crossing, the cavity is in resonance with the energy gap between the adiabatic states, S_1 and S_0, at the Franck-Condon point; in model B of Section III C, representing the spontaneous emission of the system in the vibrational ground state of S_1, the cavity is in resonance with the energy gap between S_1 and S_0 at the minima of the potentials. In both sections, we study the dynamics, first, from the viewpoint of the exact time-dependent potentials and, then, by employing CTMQC, whose accuracy is evaluated by presenting the comparison with quantum dynamics, multi-trajectory Ehrenfest dynamics and Tully surface hopping. In Section IV, we explore the possibility of reapplying the factorization idea to the marginal photon-nuclear amplitude and related time-dependent Schrödinger equation. However, due to the complexity of a "nested exact factorization" procedure, we explore at this stage only an approximate form, namely a mean-field-like factorization of the photon-nuclear wavefunction. We summarize our conclusions in Section V.

II. THEORETICAL BACKGROUND

We consider the non-relativistic photon-matter Hamiltonian, $\hat{H}_{PEN}(\boldsymbol{r},\boldsymbol{q},\boldsymbol{R})$, hereafter referred to as the photon-electron-nuclear (PEN) Hamiltonian. As described in Ref. [34], this Hamiltonian is treated within the dipole approximation in the length gauge, i.e., it is derived by applying the Power-Zienau-Woolley[87] gauge transformation to the minimal coupling Hamiltonian in the Coulomb gauge[34,62,86,88–90], resulting in

$$\hat{H}_{PEN}(\boldsymbol{r},\boldsymbol{q},\boldsymbol{R}) = \hat{H}_M(\boldsymbol{r},\boldsymbol{R}) + \hat{H}_P(\boldsymbol{q}) + \hat{H}_{PM}(\boldsymbol{r},\boldsymbol{q},\boldsymbol{R}) \quad (1)$$

with symbols $\boldsymbol{r}$ indicating the set of N_e electronic spatial coordinates, $\boldsymbol{R}$ indicating the set of N_N nuclear coordinates and $\boldsymbol{q}$ representing the displacement coordinates of the N_P cavity modes. Atomic units ($\hbar = e^2 = m_e = 1$) will be used throughout. The matter (M) Hamiltonian is the sum of the nuclear kinetic energy operator $\hat{T}_N(\boldsymbol{R})$ and of the Born-Oppenheimer (BO) Hamiltonian $\hat{H}_{BO}(\boldsymbol{r},\boldsymbol{R})$, containing the electronic kinetic energy and all the interactions $\hat{V}_{e,n}(\boldsymbol{r},\boldsymbol{R})$, namely

$$\hat{T}_N(\boldsymbol{R}) + \hat{H}_{BO}(\boldsymbol{r},\boldsymbol{R}) = \sum_{\alpha}^{N_N} \frac{-\nabla_\alpha^2}{2M_\alpha} + \sum_{i}^{N_e} \frac{-\nabla_i^2}{2} + \hat{V}_{e,n}(\boldsymbol{r},\boldsymbol{R}) \quad (2)$$

The index α labels the N_N nuclei with masses M_α and the index i is used to label the N_e electrons.

The photon Hamiltonian $\hat{H}_P(\boldsymbol{q})$, obtained through the canonical quantization of the electromagnetic field, is

$$\hat{H}_P(\boldsymbol{q}) = \hat{T}_P(\boldsymbol{q}) + \hat{V}_P(\boldsymbol{q}) = \sum_{\nu}^{2N_P} \frac{1}{2}\left(\hat{p}_\nu^2 + \omega_\nu^2 \hat{q}_\nu^2\right) \quad (3)$$

$$= \sum_{\nu}^{2N_P} \frac{-\nabla_\nu^2}{2} + \frac{1}{2}\omega_\nu^2 \hat{q}_\nu^2 \quad (4)$$

where ν labels the photon modes with frequencies ω_ν from 1 to $2N_P$ to consider the two polarizations of the electromagnetic field, i.e., of the electric and of the magnetic fields. The photon displacement operator $\hat{q}_\nu = \sqrt{\frac{1}{2\omega_\nu}}(\hat{a}_\nu^\dagger + \hat{a}_\nu)$ is related to the electric field operator, while the corresponding momentum operator $\hat{p}_\nu = -i\sqrt{\frac{\omega_\nu}{2}}(\hat{a}_\nu - \hat{a}_\nu^\dagger)$ is proportional to the magnetic field (using the symbols $\hat{a}_\nu$ and $\hat{a}_\nu^\dagger$ for the photon annihilation and creation operators). In going from Eq. (3) to Eq. (4), we expressed the photon momentum operator in position representation[37].

Finally, $\hat{H}_{PM}(\boldsymbol{r},\boldsymbol{q},\boldsymbol{R})$ represents the photon-matter interaction Hamiltonian, given by

$$\hat{H}_{PM}(\boldsymbol{r},\boldsymbol{q},\boldsymbol{R}) = \sum_{\nu}^{2N_P} \omega_\nu g_\nu \hat{q}_\nu \left(\sum_{\alpha}^{N_N} Z_\alpha \hat{\boldsymbol{R}}_\alpha - \sum_{i}^{N_e} \hat{\boldsymbol{r}}_i\right) + \frac{1}{2} g_\nu^2 \left(\sum_{\alpha}^{N_N} Z_\alpha \hat{\boldsymbol{R}}_\alpha - \sum_{i}^{N_e} \hat{\boldsymbol{r}}_i\right)^2 \quad (5)$$

where g_ν is the photon-matter coupling parameter. The second term in Eq. (5) is the self-polarization term, which depends solely on matter operators. It is worth noting that this term scales with the sum over modes of the square of the photon-matter coupling parameter, g_ν. Therefore, it is negligible in single-mode situations. Detailed discussions regarding this term can be found in Refs. [60,86].

The time evolution of the coupled PEN system is dictated by the time-dependent Schödinger equation (TDSE),

$$i\frac{\partial \Psi(\boldsymbol{r},\boldsymbol{q},\boldsymbol{R},t)}{\partial t} = \hat{H}_{PEN}(\boldsymbol{r},\boldsymbol{q},\boldsymbol{R})\Psi(\boldsymbol{r},\boldsymbol{q},\boldsymbol{R},t) \quad (6)$$

whose solution yields the time-dependent PEN wavefunction $\Psi(\boldsymbol{r},\boldsymbol{q},\boldsymbol{R},t)$ and contains the complete information about the coupled system.

Various concepts that are nowadays routinely used in the context of molecular dynamics have been generalized to PEN systems in cavities, described by the TDSE introduced above. An example is the Born-Oppenheimer approximation (BOA)[91], usually intended in the molecular framework to separate adiabatically the dynamics of the slow degrees freedom,

typically the (heavy) nuclei, to the fast degrees of freedom, like the electrons and, sometimes, the protons. The BOA assumes that the faster electrons instantaneously adapt to the positions of the nuclei; consequently, if the electrons are initialized in an eigenstate, they remain in that eigenstate as long as the BOA remains valid. It follows that the electronic eigenenergy of the occupied state delineates the BO potential energy surface (PES) that governs the nuclear dynamics. Similarly, when dealing with a PEN system, the cavity-BOA has been introduced[62] to separate the typical time-scales of the electronic degrees of freedom from those of the nuclear and photonic degrees of freedom. From the viewpoint of the quantized photon field, the cavity-BOA is physically justified by a small magnetic field since it is proportional to the momentum operator $\hat{p}_\nu$. In addition, interpreting somehow classically $\hat{p}_\nu$ as related to the time derivative of the displacement $\hat{q}_\nu$, one can assume that in the cavity-BOA the changes in time of the electric field, which is proportional to $\hat{q}_\nu$, are slow. Then, electrons can adapt "quasi-instantaneously" to these slow changes in the electric displacement field. However, rapid changes of the electric field caused by strong interaction between light and matter may lead to the breakdown of the cavity-BO approximation.

As previously done for the treatment of molecular processes beyond the BOA, we discuss here the exact factorization (EF) to go beyond the cavity-BOA. In the original formulation, the electron?nuclear wavefunction is factored as a marginal nuclear wavefunction and a conditional electronic wavefunction – conditional on the nuclear positions. However, since no approximation is made on the typical time scales of the dynamics of the two subsystems, the EF has been extended to factor different "kinds" of multicomponent many-body wavefunctions. In this work, we focus on the PEN wavefunction. Note that the choice of marginal and conditional wavefunctions is quite arbitrary but always applicable when the partial normalization condition (PNC) is imposed on the conditional term (see discussion below). Specifically, as briefly described in the Introduction, various authors have already introduced the EF formalism to analyze light-matter problems, namely electron-photon[34,35] and PEN[36] systems. Maitra and coworkers proposed $\Psi(\boldsymbol{r},\boldsymbol{q},\boldsymbol{R},t)=\chi_N(\boldsymbol{R},t)\Phi_N(\boldsymbol{r},\boldsymbol{q},t;\boldsymbol{R})=\chi_P(\boldsymbol{q},t)\Phi_P(\boldsymbol{r},\boldsymbol{R},t;\boldsymbol{q}) = \chi_E(\boldsymbol{r},t)\Phi_E(\boldsymbol{R},\boldsymbol{q},t;\boldsymbol{r})$, where the marginal amplitudes are the nuclear (N), the photonic (P) or the electronic (E) wavefunctions, respectively, and looked in some details into the first and second ideas[34]. Here, we explore an alternative possibility, where the PEN wavefunction is factored as a single product of a marginal photon-nuclear wavefunction, $\chi(\boldsymbol{q},\boldsymbol{R},t)$, and a conditional electronic wavefunction parametrically dependent on the photon-nuclear coordinates, $\Phi(\boldsymbol{r},t;\boldsymbol{q},\boldsymbol{R})$, i.e.,

$$\Psi(\boldsymbol{r},\boldsymbol{q},\boldsymbol{R},t)=\chi(\boldsymbol{q},\boldsymbol{R},t)\Phi(\boldsymbol{r},t;\boldsymbol{q},\boldsymbol{R}) \tag{7}$$

where $\Phi(\boldsymbol{r},t;\boldsymbol{q},\boldsymbol{R})$ satisfies the PNC

$$\int d\boldsymbol{r}|\Phi(\boldsymbol{r},t;\boldsymbol{q},\boldsymbol{R})|^2=1 \;\;\forall\;\; \boldsymbol{q},\boldsymbol{R},t. \tag{8}$$

As in the electron-nuclear formulation, we note that the ambiguity of the product form of the PEN wavefunction in Eq. (7) is partially eliminated by imposing this PNC, which allows us to identify the marginal photon-nuclear probability density as $|\chi(\boldsymbol{q},\boldsymbol{R},t)|^2=\int d\boldsymbol{r}|\Psi(\boldsymbol{r},\boldsymbol{q},\boldsymbol{R},t)|^2$. As a result of the PNC, the two wavefunctions are uniquely defined up to a phase factor $e^{\pm i\theta(\boldsymbol{q},\boldsymbol{R},t)}$, with $\theta(\boldsymbol{q},\boldsymbol{R},t)$ being a real function.

The TDSE for the PEN wavefunction can be rewritten using Eq. (7) along with the PNC (Eq. (8)). This leads to the following equations. The photon-nuclear TDSE is

$$i\frac{\partial\chi(\boldsymbol{q},\boldsymbol{R},t)}{\partial t}=\Bigg[\sum_\alpha\frac{(-i\nabla_\alpha+\mathbf{A}_\alpha(\boldsymbol{q},\boldsymbol{R},t))^2}{2M_\alpha} +\sum_\nu\frac{(-i\nabla_\nu+\mathbf{S}_\nu(\boldsymbol{q},\boldsymbol{R},t))^2}{2}+\varepsilon(\boldsymbol{q},\boldsymbol{R},t)\Bigg]\chi(\boldsymbol{q},\boldsymbol{R},t) \tag{9}$$

where effect of the electrons is encoded in the nuclear time-dependent vector potential ($\boldsymbol{R}$-TDVP),

$$\mathbf{A}_\alpha(\boldsymbol{q},\boldsymbol{R},t)=\langle\Phi(t;\boldsymbol{q},\boldsymbol{R})|-i\nabla_\alpha|\Phi(t;\boldsymbol{q},\boldsymbol{R})\rangle_{\boldsymbol{r}} \tag{10}$$

in the photonic time-dependent vector potential ($\boldsymbol{q}$-TDVP),

$$\mathbf{S}_\nu(\boldsymbol{q},\boldsymbol{R},t)=\langle\Phi(t;\boldsymbol{q},\boldsymbol{R})|-i\nabla_\nu|\Phi(t;\boldsymbol{q},\boldsymbol{R})\rangle_{\boldsymbol{r}} \tag{11}$$

and in the time-dependent potential energy surface (TDPES) $\varepsilon(\boldsymbol{q},\boldsymbol{R},t)$,

$$\varepsilon(\boldsymbol{q},\boldsymbol{R},t)=\varepsilon_{V_{PEN}}(\boldsymbol{q},\boldsymbol{R},t)+\varepsilon_{GD}(\boldsymbol{q},\boldsymbol{R},t)+\varepsilon_{geo}(\boldsymbol{q},\boldsymbol{R},t) \tag{12}$$

The TDPES can be written as the sum of three contributions, namely

$$\varepsilon_{V_{PEN}}(\boldsymbol{q},\boldsymbol{R},t)=\langle\Phi(t;\boldsymbol{q},\boldsymbol{R})|\hat{H}_{BO}+\hat{V}_P+\hat{H}_{PM}|\Phi(t;\boldsymbol{q},\boldsymbol{R})\rangle_{\boldsymbol{r}} \tag{13}$$

which is the gauge-invariant PEN potential,

$$\varepsilon_{geo}(\boldsymbol{q},\boldsymbol{R},t)= \sum_\alpha\frac{1}{2M_\alpha}\Big[\langle\nabla_\alpha\Phi(t;\boldsymbol{q},\boldsymbol{R})|\nabla_\alpha\Phi(t;\boldsymbol{q},\boldsymbol{R})\rangle_{\boldsymbol{r}}-\mathbf{A}_\alpha^2(\boldsymbol{q},\boldsymbol{R},t)\Big] +\sum_\nu\frac{1}{2}\Big[\langle\nabla_\nu\Phi(t;\boldsymbol{q},\boldsymbol{R})|\nabla_\nu\Phi(t;\boldsymbol{q},\boldsymbol{R})\rangle_{\boldsymbol{r}}-\mathbf{S}_\nu^2(\boldsymbol{q},\boldsymbol{R},t)\Big] \tag{14}$$

which is the gauge-invariant geometric potential, and

$$\varepsilon_{GD}(\boldsymbol{q},\boldsymbol{R},t)=\langle\Phi(t;\boldsymbol{q},\boldsymbol{R})|\,i\partial_t|\Phi(t;\boldsymbol{q},\boldsymbol{R})\rangle_{\boldsymbol{r}} \tag{15}$$

which is the gauge-dependent contribution. In Eqs. (10) to (15), the symbol $\langle\cdot\rangle_{\boldsymbol{r}}$ stands for an integration over electronic positions, and we thus removed any dependence on $\boldsymbol{r}$ of the arguments within the integral operation to show that this variable is integrated out.

The electronic evolution equation is

$$i\frac{\partial\Phi(\boldsymbol{r},t;\boldsymbol{q},\boldsymbol{R})}{\partial t}=\Big[\hat{H}_{BO}(\boldsymbol{r},\boldsymbol{R})+\hat{V}_P(\boldsymbol{q})+\hat{H}_{PM}(\boldsymbol{r},\boldsymbol{q},\boldsymbol{R}) +\hat{U}_{pen}[\Phi,\chi](\boldsymbol{q},\boldsymbol{R},t)-\varepsilon(\boldsymbol{q},\boldsymbol{R},t)\Big]\Phi(\boldsymbol{r},t;\boldsymbol{q},\boldsymbol{R}) \tag{16}$$

with the PEN coupling operator (PENCO) $\hat{U}_{pen}[\Phi,\chi](\boldsymbol{q},\boldsymbol{R},t)$ expressing the effect of the nuclei and of the photons on the electronic dynamics via its explicit dependence on $\chi(\boldsymbol{q},\boldsymbol{R},t)$. The PENCO is

$$\begin{aligned}\hat{U}_{pen}[\Phi,\chi](\boldsymbol{q},\boldsymbol{R},t) = \\ \sum_{\alpha}\frac{1}{M_\alpha}\left[\frac{(-i\nabla_\alpha-\mathbf{A}_\alpha)^2}{2}+\left(\frac{-i\nabla_\alpha\chi}{\chi}+\mathbf{A}_\alpha\right)(-i\nabla_\alpha-\mathbf{A}_\alpha)\right] \\ +\sum_{\nu}\left[\frac{(-i\nabla_\nu-\mathbf{S}_\nu)^2}{2}+\left(\frac{-i\nabla_\nu\chi}{\chi}+\mathbf{S}_\nu\right)(-i\nabla_\nu-\mathbf{S}_\nu)\right]\end{aligned} \tag{17}$$

For readability reasons we removed the dependence on $\boldsymbol{q},\boldsymbol{R},t$ of the functions on the right-hand side.

It is interesting to observe that the $\boldsymbol{R}$-TDVP and $\boldsymbol{q}$-TDVP are connected to the nuclear and photonic momentum fields, as

$$\mathbf{A}_\alpha = \frac{\mathrm{Im}[\langle\Psi(\boldsymbol{q},\boldsymbol{R},t)|\nabla_\alpha|\Psi(\boldsymbol{q},\boldsymbol{R},t)\rangle_{\boldsymbol{r}}]}{|\chi(\boldsymbol{q},\boldsymbol{R},t)|^2}-\nabla_\alpha \boldsymbol{W}(\boldsymbol{q},\boldsymbol{R},\boldsymbol{t}) \tag{18}$$

and

$$\mathbf{S}_\nu = \frac{\mathrm{Im}[\langle\Psi(\boldsymbol{q},\boldsymbol{R},t)|\nabla_\nu|\Psi\boldsymbol{q},\boldsymbol{R},t)\rangle_{\boldsymbol{r}}]}{|\chi(\boldsymbol{q},\boldsymbol{R},t)|^2}-\nabla_\nu \boldsymbol{W}(\boldsymbol{q},\boldsymbol{R},\boldsymbol{t}) \tag{19}$$

respectively. The symbol $\boldsymbol{W}(\boldsymbol{q},\boldsymbol{R},\boldsymbol{t})$ indicates the phase of the photon-nuclear wavefunction $\chi(\boldsymbol{q},\boldsymbol{R},t)$, has the dimensions of an action and is related to the gauge phase $\theta(\boldsymbol{q},\boldsymbol{R},t)$ introduced above. In this work, the gauge for the quantum dynamics calculations will be chosen such that the photon-nuclear wavefunction is always non-negative and real, namely $\chi(\boldsymbol{q},\boldsymbol{R},t) = +\sqrt{\int d\boldsymbol{r}|\Psi(\boldsymbol{r},\boldsymbol{q},\boldsymbol{R},t)|^2}$, meaning that $\boldsymbol{W}(\boldsymbol{q},\boldsymbol{R},\boldsymbol{t}) = 0$. In this particular gauge, Eqs. (18) and (19) show that the TDVP becomes the nuclear and the photonic momentum fields, respectively.

The EF of the PEN wavefunction just derived naturally lends itself to a mixed quantum-classical treatment in the spirit of the analogous approach derived for the electron-nuclear problem. Here, we aim to treat on equal footing the photonic and the nuclear degrees of freedom, by introducing the idea of photon-nuclear trajectories, whereas the electrons are described quantum mechanically. Therefore, we will now briefly describe how the CTMQC algorithm can be easily extended to the PEN problem in Section II A, and we will test it in Section III on two model case studies of dynamical processes in the strong light-matter coupling regime.

A. Coupled-trajectory mixed quantum-classical algorithm

Building upon the developments of CTMQC from EF to treat processes beyond the BOA in electron-nuclear systems using trajectory-based on-the-fly dynamics[9–11], we propose here to extend the applicability of the algorithm to study situations beyond the cavity-BOA using coupled trajectories to describe the photon-nuclear dynamics under the effect of quantum-mechanical electrons.

The photon-nuclear dynamics of Eq. (9) will be solved via an ensemble of *coupled trajectories* representing both nuclei and photons, thus, they will be indicated as $\boldsymbol{q}_I(t),\boldsymbol{R}_I(t) = \boldsymbol{X}_I(t)$. To simplify the notation below, we will indicate the dependence on the photon-nuclear trajectories only via the label I; each trajectory at every time thus becomes a collection of N_N+2N_P coordinates, that will be collectively labeled with the index $\Gamma\equiv\alpha,\nu$. The evolution of positions and momenta of these trajectories adheres to Hamilton's equations of motion, guided by the TDPES, the $\boldsymbol{R}$-TDVP, and the $\boldsymbol{q}$-TDVP.

In CTMQC, the electronic wavefunction is expanded in the cavity-adiabatic basis,

$$\Phi(\boldsymbol{r},t;\boldsymbol{q},\boldsymbol{R}) = \sum_k C_k(\boldsymbol{q},\boldsymbol{R},t)\phi_k(\boldsymbol{r};\boldsymbol{q},\boldsymbol{R}) \tag{20}$$

with $\phi_k(\boldsymbol{r};\boldsymbol{q},\boldsymbol{R})$ the set of eigenstates of the Hamiltonian $\hat{V}_{PEN}(\boldsymbol{q},\boldsymbol{R}) = \hat{H}_{PEN}(\boldsymbol{r},\boldsymbol{q},\boldsymbol{R}) - \hat{T}_N(\boldsymbol{R}) - \hat{T}_P(\boldsymbol{q})$, with eigenvalues $E_k(\boldsymbol{q},\boldsymbol{R})$, representing the electronic PESs as functions of the photonic and nuclear coordinates. The nonadiabatic couplings between two of these electronic states encode the information on the variation along $\boldsymbol{R}$ (∇_α) or along $\boldsymbol{q}$ (∇_ν) of the states; they will be indicated collectively as $\boldsymbol{d}_{kl,\Gamma}(\boldsymbol{q},\boldsymbol{R}) = \left\langle\phi_k(\boldsymbol{q},\boldsymbol{R})|\nabla_\Gamma|\phi_l(\boldsymbol{q},\boldsymbol{R})\right\rangle_{\boldsymbol{r}}$.

Inserting Eq. (20) into Eq. (16) and introducing some approximations, as described previously for CTMQC and its various flavours[17,92], yields the evolution equations for the electronic coefficients along each trajectory I

$$\dot{C}_k^{(I)}(t) = \dot{C}_{k,Eh}^{(I)}(t) + \dot{C}_{k,CT}^{(I)}(t) \tag{21}$$

The first term in the right-hand side is a standard Ehrenfest-like (*Eh*) term

$$\dot{C}_{k,Eh}^{(I)}(t) = -iE_k^{(I)}C_k^{(I)}(t) - \sum_\Gamma \boldsymbol{V}_\Gamma^{(I)}(t)\cdot\sum_l \boldsymbol{d}_{kl,\Gamma}^{(I)}(\boldsymbol{R})C_l(t) \tag{22}$$

whereas the second term, i.e. the *coupled-trajectory* (*CT*) term, reads

$$\dot{C}_{k,CT}^{(I)}(t) = \sum_\Gamma \frac{\mathscr{P}_\Gamma^{(I)}(t)}{M_\Gamma}\cdot\left(\boldsymbol{f}_{k,\Gamma}^{(I)} - \sum_l |C_l^{(I)}(t)|^2\boldsymbol{f}_{l,\Gamma}^{(I)}\right)C_k(t) \tag{23}$$

In Eqs. (22) and (23), we have introduced the new symbols: $\boldsymbol{V}_\Gamma^{(I)}(t) = \dot{\boldsymbol{X}}_\Gamma^{(I)}(t)$ standing for the velocity of the trajectory I, $\mathscr{P}_\Gamma^{(I)}(t) = -\nabla_\Gamma|\chi^{(I)}(t)|^2/(2|\chi^{(I)}(t)|^2)$ representing the quantum momentum, and $\boldsymbol{f}_{k,\Gamma}^{(I)} = \int_0^t(-\nabla_\Gamma E_k^{(I)})d\tau$ being the cavity-adiabatic forces accumulated along the trajectory I.

The classical nuclear force that generates the trajectory I can be derived from Eq. (9) as described for instance in Ref. [93], and reads

$$\boldsymbol{F}_\Gamma^{(I)}(t) = \boldsymbol{F}_{\Gamma,Eh}^{(I)}(t) + \boldsymbol{F}_{\Gamma,CT}^{(I)}(t) \tag{24}$$

The first term in the right-hand side is a mean-field, or Ehrenfest-like, term

$$\boldsymbol{F}^{(I)}_{\Gamma,Eh}(t) = -\sum_k |C^{(I)}_k(t)|^2 \nabla_\Gamma E^{(I)}_k - \sum_{k,l} \bar{C}^{(I)}_l(t) C^{(I)}_k(t) (E^{(I)}_k - E^{(I)}_l) \boldsymbol{d}^{(I)}_{kl,\Gamma} \tag{25}$$

whereas the second term is, similarly to the electronic equation, a coupled-trajectory (CT) term

$$\boldsymbol{F}^{(I)}_{\Gamma,CT}(t) = \sum_{k,l} \sum_{\Gamma'} \left(\mathscr{P}^{(I)}_{\Gamma'} \cdot \boldsymbol{f}^{(I)}_{k,\Gamma'} \right) \left(\boldsymbol{f}^{(I)}_{k,\Gamma} - \boldsymbol{f}^{(I)}_{l,\Gamma} \right) |C^{(I)}_k(t)|^2 |C^{(I)}_l(t)|^2 \tag{26}$$

Note that in Eq. (25), we introduced the symbol $\bar{C}^{(I)}_l(t)$ to indicate the complex conjugate of $C^{(I)}_l(t)$.

As in the usual formulation of CTMQC, the photon-nuclear density $|\chi^{(I)}(t)|^2$ is reconstructed as a sum of frozen Gaussians centered at the positions of the trajectories. This calculation requires that, at the end of each dynamics step, the trajectories share information about their positions to compute the quantum momentum. Once the quantum momentum is determined, the trajectories can proceed with a new step of dynamics. On-the-fly calculation of the quantum momentum is feasible only when the trajectories are propagated simultaneously, that is why the underlying algorithm has been dubbed "coupled-trajectory"-MQC. Incorporating information about the delocalization of classical trajectories enhances the description of nonadiabatic effects, i.e., due to the electronic excited states, and of quantum effects, compared to methods such as multi-trajectory Ehrenfest (MTE) or Tully surface hopping (TSH).

The CTMQC algorithm, as presented in this section, is a straightforward extension of the electron-nuclear case, which requires a classical-like trajectory-based treatment of the photons as well as of the nuclei. The photons are simply represented by additional degrees of freedom to those representing the nuclei.

To illustrate the advantage of such an approach in comparison to the, perhaps more standard, polaritonic picture, let us consider a simple scenario involving a system with one nucleus, one photonic mode, and two electronic states. In our formulation, we would propagate the photon and nucleus classically using coupled trajectories under the effect of the two electronic states. Alternatively, if we were to adopt a different EF form of the PEN wavefunction, for instance $\chi_N(\boldsymbol{R},t)\Phi_N(\boldsymbol{r},\boldsymbol{q},t;\boldsymbol{R})$, where the nuclear wavefunction is the marginal amplitude and the photon-electronic wavefunction is the conditional amplitude, the two electronic states would be dressed by the photons, yielding the polaritonic states. The mixing of the electronic and photonic degrees of freedom would yield at least four polaritonic states, if one were to consider only the zero-photon and one-photon states. The one-dimensional nuclear evolution then takes place under the effect of these four polaritonic states. This alternative representation, while conceptually interesting and widely used in the literature, might prove computationally more demanding for the CTMQC algorithm as well as for the coupled-trajectory Tully surface hopping (CTTSH) algorithm[18] – derived as well from EF. Specifically, CTMQC requires the calculation of nonadiabatic coupling vectors at all times to evaluate nuclear forces, while both CTMQC and CTTSH require calculations of nuclear gradients of the cavity-adiabatic/polaritonic PESs at all times to evaluate the force accumulated along the trajectories. Thus, treating four polaritonic states instead of two electronic states is clearly more expensive from the computational perspective. Furthermore, we stress that we are not pioneering the idea of treating photons in terms of trajectories; other authors have utilized such an idea, for instance in the context of the vibrational strong-coupling regime[56,65].

III. NUMERICAL APPLICATIONS

In this section, we discuss the PEN problem in two different physical conditions employing low-dimensional model Hamiltonians. The system comprises one nuclear mode and two singlet electronic states, S_0 and S_1, and it is coupled to a single-mode cavity. Model *A* represents a typical nonadiabatic situation with the adiabatic PESs forming an avoided crossing at some nuclear geometries, and the cavity is in resonance with the S_0-to-S_1 transition at the Franck-Condon point. In this case, we will study the effect of the cavity on the relaxation process of the initially photoexcited system. Model *B* is constructed to induce the spontaneous photon emission of the system from S_1 to S_0, followed by photoexcitation due to the absorption of the emitted photon. In this case, the cavity is in resonance with the S_0-to-S_1 energy gap at the minimum of the S_1 PES.

In the used models we have $\alpha = 1$ and $\nu = 1$, then the kinetic energies are $\hat{T}_N = -(2M)^{-1}\partial^2_R$, with $M = 20000\ \mathrm{m}_e$, and $\hat{T}_P = -\partial^2_q$. The BO Hamiltonian in the diabatic basis is

$$\hat{H}_{BO}(\boldsymbol{R}) = \begin{pmatrix} \frac{1}{2}k(R-R_1)^2 & b\exp\left[-a(R-R_3)^2\right] \\ b\exp\left[-a(R-R_3)^2\right] & \frac{1}{2}k(R-R_2)^2 + \Delta \end{pmatrix} \tag{27}$$

The diagonal elements are two parabolas displaced in position, at R_1 and R_2, and in energy, by Δ, with Gaussian off-diagonal couplings centered at R_3. In the same basis, the Hamiltonian $\hat{V}_{PEN}$ is

$$\hat{V}_{PEN}(\boldsymbol{q},\boldsymbol{R}) = \hat{H}_{BO}(\boldsymbol{R}) + \begin{pmatrix} \frac{1}{2}\omega^2 q^2 + Z\omega g q R & -\omega g \mu_{12} \\ -\omega g \mu_{12} & \frac{1}{2}\omega^2 q^2 + Z\omega g q R \end{pmatrix} \tag{28}$$

In this expression, we have omitted the second term in Eq. (5), i.e., the self-polarization term, which is usually negligible when considering a single-mode cavity. We confirmed this by including this term in our numerical calculations, and indeed its presence did not contribute significantly to the results. In Eq. (28), our model is defined such that the diagonal elements of dipole operator in the diabatic basis are zero and the off-diagonal elements, i.e., the transition dipole moment, is a constant function of nuclear geometries of value $\mu_{12} = 1.0\ \mathrm{ea}_0$ (Condon approximation). Furthermore, we choose $Z = 1.0$ e.

A. Computational details

Quantum dynamics (QD) simulations are performed in the diabatic basis using the split-operator technique on a grid of 500×500 points in the range $q \in [-10, 10]$ a$_0$ and $R \in [0, 8]$ a$_0$. We used a time step $dt = 0.05$ a.t.u. These calculations provide the full PEN wavefunction in the electronic diabatic basis with corresponding photon-nuclear amplitudes. The marginal photon-nuclear density of the EF is then calculated as well as the electronic conditional amplitude in the diabatic basis. The TDPES and the TDVP can be calculated using the electronic amplitude as illustrated in detail in Ref. [7]. The initial state of the system for both models studied here is defined with full occupation of the S_1 state and with a Gaussian in q and in R centered at $q = 0$ and $R = 2$ a$_0$. The widths of the Gaussians are $\sigma_q = 2.425$ a$_0$ and $\sigma_R = 0.223$ a$_0$.

Trajectory-based simulations are performed in the cavity-adiabatic basis, which we define as the representation where Eq. (28) is diagonal. The model Hamiltonians of Eqs. (27) and (28) have been implemented in the QuantumModelLib library[94]. The G-CTMQC code[95] used for all the trajectory-based simulations is interfaced with QuantumModelLib, providing energies, gradients and couplings on-th-fly upon diagonalization of the diabatic Hamiltonian. In G-CTMQC the trajectory-based simulations are performed by solving the photon-nuclear equations with the velocity-Verlet algorithm and the electronic equations with the Runge-Kutta-Gill algorithm. The time step is $dt = 0.1$ a.t.u., for both photon-nuclear and electronic dynamics. An ensemble of 10000 trajectories were considered for all the calculations presented. The initial positions and momenta are sampled from the (harmonic) quantum distribution determined as the Wigner transform of the initial photon-nuclear probability density used in QD calculations.

B. Nonadiabatic dynamics: Model *A*

Figure 1 shows cuts of the two-dimensional PESs obtained by diagonalizing the Hamiltonian of Eq. (28), with the following parameters (in atomic units): $k = 0.020$ E$_h^2$m$_e/\hbar^2$, $a = 3.0$ a$_0^{-2}$, $b = 0.01$ E$_h$, $\Delta = 0$, $R_1 = 6.0$ a$_0$, $R_2 = 2.0$ a$_0$, and $R_3 = 3.875$ a$_0$. The cuts of the cavity-adiabatic PESs of Fig. 1 are given as functions of R in the left panels for $q = 0$ and $q = 1.5$ a$_0$ and as functions of q in the right panels for $R = 2.0$ a$_0$ and $R = 4.0$ a$_0$ (which are, respectively, the minimum of one of the two parabolas where the initial wavepacket is centered and the center of the nonadiabatic region). Note that top panels in Fig. 1 show, for reference, the shapes of the PESs in the absence of coupling between the system and the cavity, while the bottom panels provide an idea of how the PESs are modified by the strong coupling between the system and the cavity. In all cases, the PESs as functions of R for given values of q represent a ground-state double-well potential and an excited-state single well. By tuning the parameters of the model, namely the resonance frequency ω and the coupling strength g, we can induce different dynamics, since the potentials that drive the evolution of the system are slightly

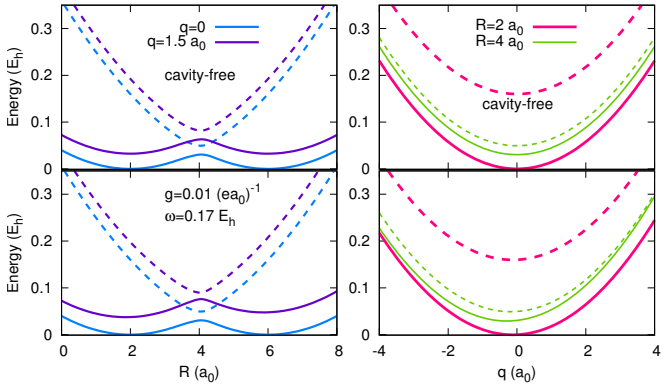

FIG. 1. Left: Cuts of the cavity-adiabatic PESs as function of R along $q = 0$ (light-blue) and $q = 1.5$ a$_0$ (purple), for the cavity-free case (upper panels) and for the strong-coupling case (lower panels). Right: Cuts of the cavity-adiabatic PESs as function of q along $R = 2$ a$_0$ (fuchsia) and $R = 4$ a$_0$ (light-green), for the cavity-free case (upper panels) and for the strong-coupling case (lower panels). Continuous lines are used for the electronic ground state S_0 and dashed lines for the excited state S_1.

s

modified, as shown in Fig. 1. In the cases studied below, and as indicated above, ω is chosen such that the cavity is in resonance with the S_0-to-S_1 excitation at the Franck-Condon point $R = 2$ a$_0$, $q = 0$. On the other hand, as function of q, the cavity-adiabatic PESs are basically parabolas more or less symetric with respect to $q = 0$ depending on the coupling g.

Exact QD simulations were conducted starting with an initial wavepacket in the excited state, represented as a real two-dimensional Gaussian centered at $R = 2.0$ a$_0$ and $q = 0$: this means that the system, which is in the vibrational ground state of the left diabatic well, is photoexcited at the initial time in a cavity with zero photons. In the course the dynamics, depending on the coupling strength and on the resonance frequency, photon emission and nonadiabatic population transfer take place. Specifically, the cavity-free dynamics for $g = 0$ would be characterized by a nonadiabatic event that takes place when the wavepacket reaches the avoided crossing region, without photon-emission events. Instead, in the strong light-matter coupling regime, achieved with $g = 0.01$ (ea$_0$)$^{-1}$ and $\omega = 0.17$ E$_h$ in our calculations, the cavity is in resonance with the excitation of the system in the Franck-Condon region, thus, as soon as the nonadiabatic dynamics starts, photon-emission is observed. In order to quantify the photon-emission process, we will calculate the expectation value of photon number operator, namely

$$\langle \hat{N} \rangle = \langle \hat{a}^\dagger \hat{a} \rangle = \frac{\omega}{2} \langle \hat{q}^2 \rangle + \frac{1}{2\omega} \langle \hat{p}^2 \rangle - \frac{1}{2} \qquad (29)$$

that we have expressed in terms of the photon displacement operator and corresponding momentum (as mentioned earlier there is no contribution from the self-polarization term in this model).

For the cavity-free dynamics, the population of the S_1 state is shown for reference in Fig. 2. In this case, the dynamics is purely nonadiabatic without photon-emission,

thus radiative decay is not permitted. However, the non-radiative decay appears starting at $t = 800$ a.t.u., when the photoexcited wavepacket approaches the avoided crossing at $R = 4$ a_0, where nonadiabaticity is the strongest. At around $t = 1050$ a.t.u., the S_1 population increases again, since the wavepacket is being reflected by the right wall of the potential and goes back towards the avoided crossing. Figure 2 reports the time trace of the S_1 population for the cavity-free dynamics calculated via QD (black line) as well as the trajectory-based results that will be discussed below.

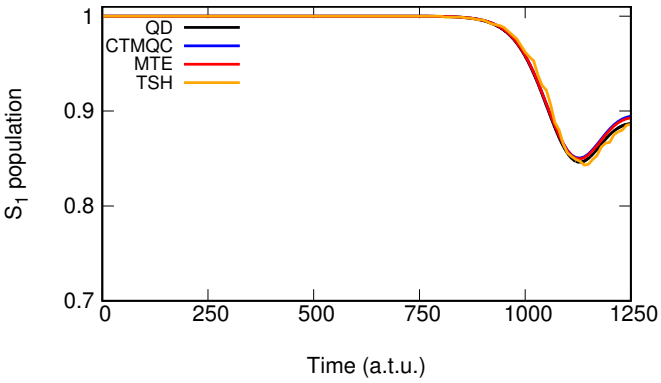

FIG. 2. S_1 population as function of time for cavity-free dynamics. QD results are shown in black and three different trajectory-based approaches are compared: CTMQC in blue, MTE in red and TSH in orange.

In the strong-coupling regime, which will be investigated further below, the coupling between the system and the cavity is strong since the beginning of the simulated dynamics, and leads to an immediate photon-emission event: the S_1 population decreases while the number of photons increases. Shortly after $t = 400$ a.t.u., the average number of photons stabilizes at approximately 0.15. At around $t = 1000$ a.t.u., the S_1 population decreases again since the S_1 wavepacket decays non-radiatively via the avoided crossing.

1. *Time-dependent potentials*

In this section, we analyze the time-dependent potentials of the exact factorization, namely the TDPES, the $\boldsymbol{R}$-TDVP, and $\boldsymbol{q}$-TDVP introduced in Sec. II, aiming to relate their features to the behavior of the photon-nuclear density.

In Fig. 3, the TDPES is represented at different snapshots along the dynamics as color map with the superimposed black contour lines indicating the photon-nuclear density.

At $t = 0$, the TDPES reproduces the shape of the cavity-adiabatic S_1 PES, where the photoexcited wavepacket is initially prepared: its slope in the R direction induces the density to move towards the right, while it confines the density in the q direction being essentially a parabola. While the dynamics of the photon-nuclear density is quite simple, as it mainly moves in R towards the right, we can observe that an interesting behavior develops in time along q. Around $t = 500$ a.t.u., the TDPES modulates its shape between $R = 2$ a_0 and $R = 2.5$ a_0, causing the density to separate in two portions, one that moves to the right and one that remains in the Franck-Condon region all along the dynamics. In the Franck-Condon region, we observe the formation of a localized peak extending in the R direction up to (slightly less than) $R = 2.5$ a_0 at $q = 0$, which enforces the splitting of the photon-nuclear density along q. There, the shape of the density along q is reminiscent of the first excited state of the harmonic potential, thus it coincides with the photon formation. The formation of the two portions of the density along R is complete already at $t = 750$ a.t.u., and at later times, i.e., $t = 1000$ a.t.u. in the figure, while the S_1 component continues its evolution towards the avoided crossing, the component associated to the Franck-Condon region remains fairly well localilzed on the left. At the final snapshot reported, namely at $t = 1250$ a.t.u., a very small portion of density moving towards the right remains in the excited state after the passage through the avoided crossing, and is reflected back (not visible in the panel), while the main portion keeps travelling in the ground state towards the right.

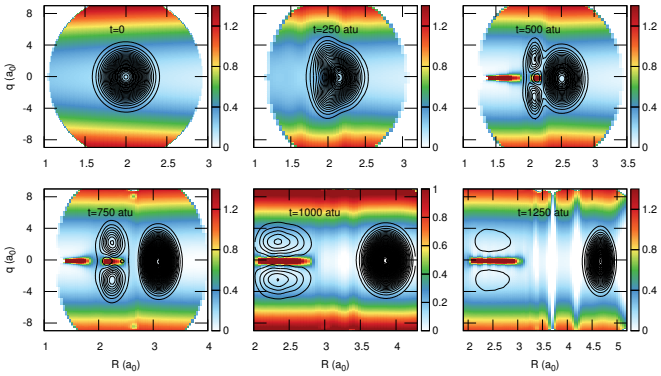

FIG. 3. TDPES for model A at times: $t = 0, 250, 500, 750, 1000, 1250$ a.t.u., as indicated in the panels. The color bar is given in hartree. The nuclear density is superimposed at the same times as black contour lines.

Cuts of the TDPES are reported in Fig. 4 at times $t = 250, 750, 1250$ a.t.u. (as indicated in the panels) and can be analyzed by superimposing them to the cuts of the cavity-adiabatic PESs reported in Fig. 1.

In the left panels of Fig. 4, the one-dimensional TDPES is plotted for $q = 0$ (orange circles) and for $q = 1.5$ a_0 (green circles) as function of the nuclear coordinate R. Note that the orange and green circles represent only the component $\varepsilon_{V_{PEN}}(q,R,t)$ of the full TDPES. For the same values of q, we report cuts of the photon-nuclear density as functions of R (thin orange and green lines). In agreement with the above discussion, we observe that at the times reported in the figure, the density develops two main portions. The portion that remains in the Franck-Condon region (at around $R = 2$ a_0) is partially associated to the electronic ground states and partially to the excited state. Specifically, the shape of the TDPES in orange (for $q = 0$) follows at all times reported in the figure the shape of the excited state (dashed lines), while the shape of the TDPES in green (for $q = 1.5$ a_0) at $t = 1250$ a.t.u. follows the ground state (continuous lines). The portion of the density that moves towards the avoided crossing under-

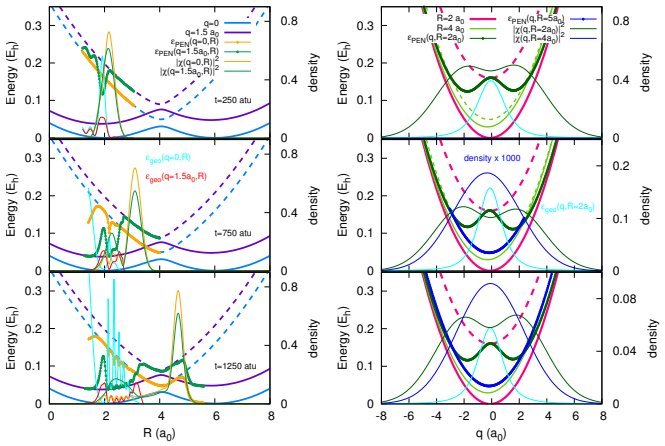

FIG. 4. Left: Cuts of the TDPES as function of R at times $t = 250, 750, 1250$ a.t.u., decomposed in $\varepsilon_{V_{PEN}}(q,R,t)$ (orange circles at $q = 0$ and green circles at $q = 1.5$ a$_0$) and in $\varepsilon_{geo}(q,R,t)$ (cyan lines at $q = 0$ and red lines at $q = 1.5$ a$_0$) and superimposed at the cavity-adiabatic PESs (purple and light-blue as in Fig. 1). Thin orange and green lines are the corresponding cuts of the photon-nuclear density as functions of R along the same values of q. Right: Cuts of the TDPES as function of q, decomposed in $\varepsilon_{V_{PEN}}(q,R,t)$ (dark-green circles at $R = 2$ a$_0$ and blue circles at $R = 4$ a$_0$) and in $\varepsilon_{geo}(q,R,t)$ (cyan at $R = 2$ a$_0$) and superimposed at the cavity-adiabatic PESs (fuchsia and light-green as in Fig. 1). Thin dark-green and blue lines are the corresponding cuts of the photon-nuclear density as functions of q along the same values of R. Note that in the top panel the thin blue line is not visible because at $R = 4$ a$_0$ at $t = 250$ a.t.u. the density is nearly zero.

goes a nonadiabatic population transfer at around $R = 4$ a$_0$, and evolves as well partially in the excited state and partially in the ground state since the TDPES develops a characteristic step that bridges between the cavity-adiabatic shapes of the (static) PESs. The geometric component of the TDPES, namely $\varepsilon_{geo}(q,R,t)$ represented in cyan and in red in Fig. 4, develops a strongly oscillatory behavior only in the Franck-Condon region, that is partially responsible for the oscillations observed as well in the density. The oscillations in $\varepsilon_{geo}(q,R,t)$ as function of R for fixed q, however, do not strongly affect the overall shape of the density, only its fine interference patterns.

Interestingly, as also previously discussed by Maitra and coworkers[34,38], the TDPES as a function of q for two different values of the nuclear coordinate, namely $R = 2$ a$_0$ (dark-green circles) and $R = 4$ a$_0$ (blue circles), can become strongly anharmonic. At all times reported in Fig. 4, for $R = 2$ a$_0$, the component $\varepsilon_{V_{PEN}}(q,R,t)$ of TDPES develops a barrier around $q = 0$ whose maximum value reaches the corresponding electronic excited state. In addition, the geometric component ε_{geo} that is summed to $\varepsilon_{V_{PEN}}$ to obtain the full TDPES, presents as well a high broad barrier centered in $q = 0$ for $R = 2$ a$_0$ (note that for $R = 4$ a$_0$, ε_{geo} is a nearly constant function of q with a small negative value that is not reported in Fig. 4). The analysis of the cuts of the TDPES allows us to conclude that as function of q the TDPES is strongly anharmonic, despite the fact that the cavity-adiabatic electronic PESs are seemingly harmonic, and that its shape is strongly dominated by ε_{geo}.

In the chosen gauge for the QD calculations, the $\boldsymbol{R}$-TDVP is the nuclear momentum field and the $\boldsymbol{q}$-TDVP is the photon momentum field. Thus, they provide additional insights into the photon-nuclear dynamics, complementing the information derived from the TDPES. However, the details of the photon momentum filed are obscured in the total TDVP due to the chosen larger mass associated to the nuclear degree of freedom than that of the photon displacement (20000 times larger). This causes the TDVP in the R-direction to be dominant. Therefore, rather than showing the momentum field, in Fig. 5 we show the velocity field: the color map provides information about the modulus of the velocity vector field while the unit-vectors about its direction.

In Fig. 5, at the initial time, $t = 0$, the system is initialized with the zero momentum in the R direction and is in the ground state along the q direction, thus the velocity field is very small everywhere. Afterwards, the photon-nuclear density (depicted in all panels as black contour lines) starts mainly to move towards the right in the R direction. However, since we are showing the velocity field in the figure, we are able to clearly observed all along the dynamics, at all snapshots reported in Fig. 5, that the field changes direction often along q, and while one portion of the density moves away from the Franck-Condon region towards the right in R, the density rapidly oscillates "up and down" along the q direction. As the portion of the density moving towards the right in R approaches the avoided crossing, it gains velocity, and the nuclear component begins to be relevant, as indicated at $t = 500$ a.t.u. onwards. However, the oscillations in the q direction persist, and the arrows keep changing direction.

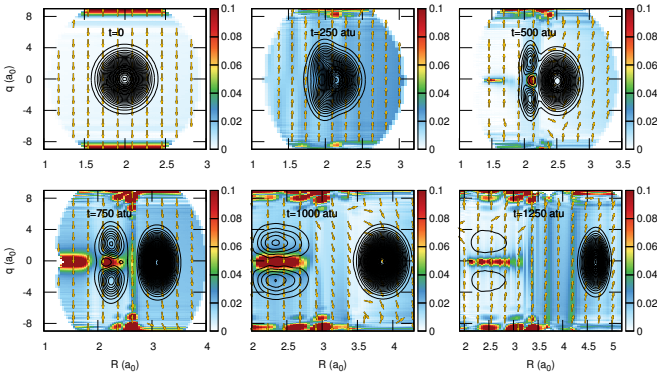

FIG. 5. Photon-nuclear velocity field for model A at times: $t = 0, 250, 500, 750, 1000, 1250$ a.t.u. as indicated in the panels. The color map indicates the squared modulus of the velocity field in $[a_0 E_h/(\hbar m_e)]^2$ and the unit-vectors (arrows) show the orientation of the velocity field. The nuclear density is superimposed as black contour lines at the corresponding times.

2. *CTMQC dynamics*

In this section, we test the performance of the trajectory-based treatment of the coupled PEN dynamics just described, using CTMQC. This study extends the classical-like treatment

that uses coupled trajectories to the photon displacement coordinate and momentum, treating the photons essentially as additional nuclear-like degrees of freedom of the system.

The classical-like coordinates R and q, along with their conjugate momenta, define the phase-space coordinates. An ensemble of initial conditions is sampled based on the photon-nuclear density time $t = 0$ used in the QD simulations above, while the electronic system is in its excited state. Then, the phase-space variables along with the electronic coefficients are propagated using CTMQC equations. Below, we will show results obtained using CTMQC as well as the multi-trajectory Ehrenfest (MTE) method and Tully surface hopping (TSH), in order to evaluate the performance of CTMQC in comparison with other similar approaches in addition to benchmark the trajectory-based dynamics against QD simulations.

In Fig. 6, we present in the top panel the evolution of the expectation value of the photon number $\langle \hat{N} \rangle$ and in the bottom panel the time trace of the electronic population in the excited state S_1. In the figure, the reference QD results are in black, CTMQC is in blue, MTE in red and TSH in orange. We remind that we used here the parameters $\omega = 0.17$ E_h and $g = 0.01$ $(ea_0)^{-1}$; the photon-nuclear density is centered initially at $R = 2.0$ a_0 and $q = 0.0$ a_0. Since the cavity is in

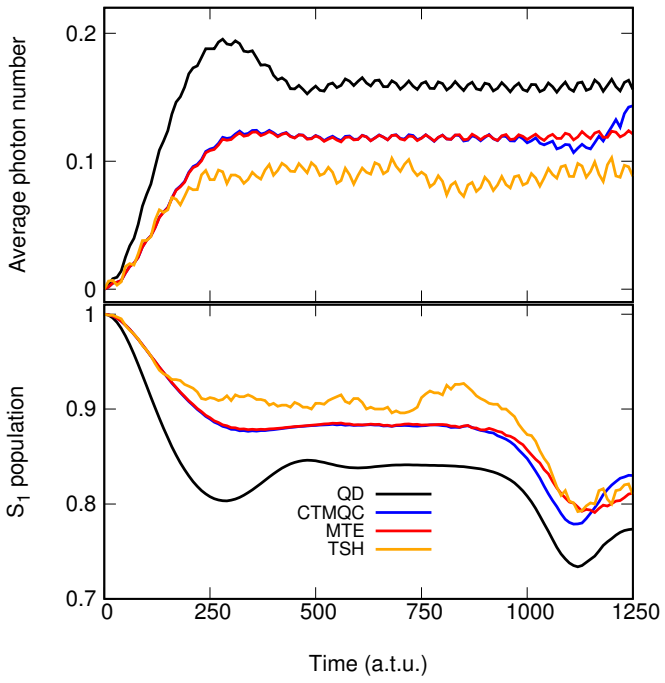

FIG. 6. Top: Average photon number as function of time. Bottom: S_1 population as function of time. QD results are shown in black and three different trajectory-based approaches are compared: CTMQC in blue, MTE in red and TSH in orange.

resonance with the S_0-to-S_1 transition at the Franck-Condon point, where the dynamics starts, electronic population is immediately transferred from the excited state to the ground state by emitting photons, as the initial increase of the average photon number confirms. All trajectory methods underestimate these effects, i.e., the transfer of population and the creation of photons. However, CTMQC and MTE agree better with the reference than TSH. Overall, the fast oscillations of the average photon number, related to the oscillation of the velocity field along q discussed above in Fig. 5, are well-captured by CTMQC and MTE, while they appear to be unstable in TSH.

We suppose that CTMQC underestimates the initial increase in the photon number, and thus the population transfer, due to the complete neglect of the term ε_{geo} in the TDPES and the corresponding contribution in the electronic evolution equation. This term contains second-order derivatives with respect to the photon-nuclear coordinate, which are expensive to compute numerically. In addition, it has been shown that it is indeed negligible when analyzing the EF factorization in terms of the (small) electron-nuclear mass ratio[96]. In our PEN problem, this argument is invalid, and such term becomes important, or even dominant, as shown, for instance, in Fig. 4. The absence of this term prevents the approximated TDPES to develop a strong barrier around $q = 0$ in the Franck-Condon region, thus the distribution of trajectories cannot fully reproduce the QD density, with a shape that is reminiscent of the first excited state of the harmonic oscillator. This observation is supported by the results shown in Fig. 2, where CTMQC (blue line) – as well as MTE (red line) and TSH (orange line) – perfectly agrees with QD results (black line) in the cavity-free case where the nonadiabatic dynamics of the electron-nuclear system is not affected by the strong coupling to the cavity. In Refs. [34,38], a similar behavior of the TDPES and of ε_{geo} was observed, even though the factorization of the system was done in a different way. There, the PEN wavefunction was expressed as $\Psi(\boldsymbol{r},\boldsymbol{q},\boldsymbol{R},t) = \chi_E(\boldsymbol{q},t)\Phi_E(\boldsymbol{r},\boldsymbol{R},t;\boldsymbol{q})$, and the ε_{geo} showed a similar and significant contribution to the total TDPES. This leads us to conclude that ε_{geo} should be considered for further improvements in CTMQC to enhance the photon description.

The similarities observed in Fig. 6 between CTMQC and MTE suggest that, for model A, the mean-field component of the coupling between the photon-nuclear degrees of freedom and the electrons is the leading effect in CTMQC. However, in CTMQC, the coupling of the trajectories, encoded in the quantum momentum, affects both the photon-nuclear and the electronic dynamics. Its effect becomes evident in Fig. 7, where we show the marginal nuclear densities at times $t = 0, 500, 1250$ a.t.u. as indicated in the figure, for CTMQC (top panels), MTE (middle panels), and TSH (bottom panels). The superimposed solid black lines are the reference marginal nuclear densities of QD calculations. From the comparison of methods reported in Fig. 6, it is clear that, even if not with perfect agreement with QD, CTMQC is able to reproduce better the splitting of the marginal nuclear density observed at long times. Finally, note that in model A, there is not significant information to be derived from the photonic marginal density as it remains close to a Gaussian centered at $q = 0$ throughout the dynamics, providing limited insights.

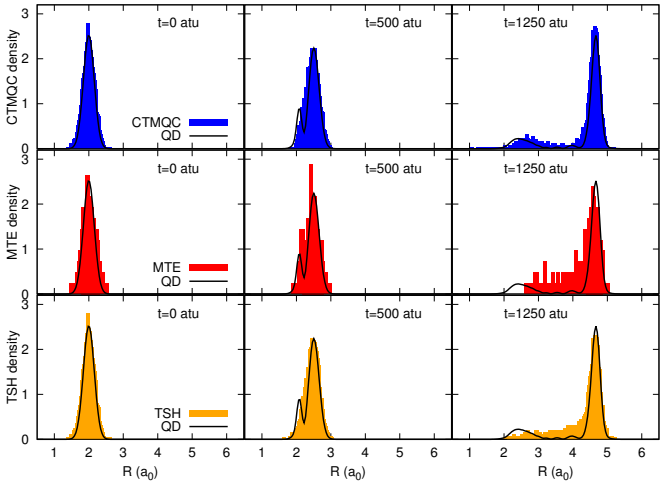

FIG. 7. In colours, the histograms represent the distributions of trajectories aiming to reproduce the marginal nuclear densities for model *A* calculated with CTMQC (blue), MTE (red), and TSH (orange) at times $t = 0, 500, 1250$ a.t.u.; the QD marginal nuclear density is shown as black lines at the same times.

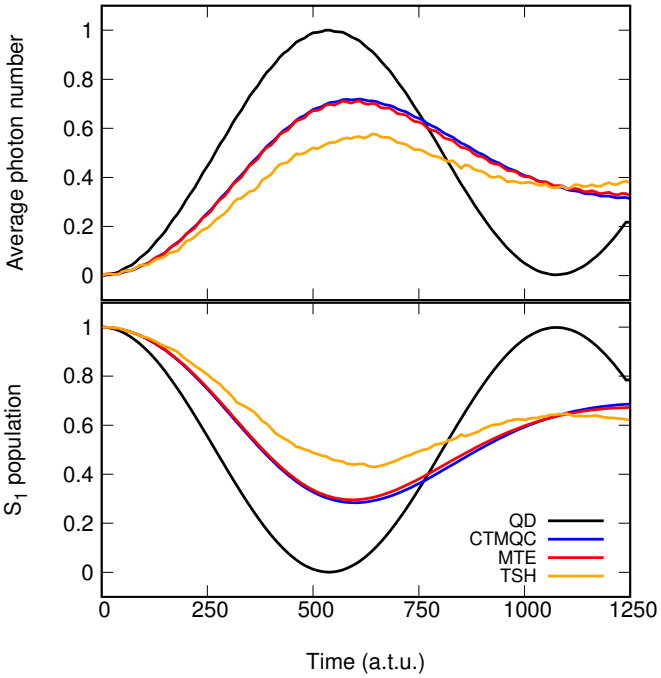

FIG. 8. Same as Fig. 6 but for model *B*.

C. Spontaneous emission: Model *B*

Model *B* reproduces a situation of spontaneous emission due to the strong coupling between the system, initially in the vibrational ground state of the electronic excited state S_1, and the cavity, that is resonance with the S_1-to-S_0 transition at the minimum of the S_1 PES. We use the Hamiltonians of Eqs. (28) and (27), with parameters: $k = 0.020\ E_h^2 m_e/\hbar^2$, $a = 3.0\ a_0^{-2}$, $b = 0.01\ E_h$, $\Delta = 0.17\ E_h$, $R_1 = 2.0\ a_0$, $R_2 = 2.0\ a_0$, $R_3 = 3.875\ a_0$. The coupling between the system and the cavity is encoded in $\omega = 0.17\ E_h$ and in $g = 0.01\ (ea_0)^{-1}$.

QD simulations were performed by initializing the system in the excited state as a Gaussian photon-nuclear wavepacket center at $R = 2.0\ a_0$ and $q = 0$ with zero momentum. Since the system starts in the lower vibrational level of the electronic excited state and the nonadiabatic coupling to the ground state is negligible, the only possible decay pathway is via a radiative decay, achievable within the time of our simulations in the strong-coupling regime.

The average photon number as function of time along with the time trace of the population of the excited state S_1 are shown in Fig. 8. From the QD results (black lines), we observe that photon emission and population transfer occur simultaneously, and in this case the average photon number reaches unity when the electronic population is fully in the ground state. After that, the photon is fully reabsorbed by the system that goes back entirely in the excited state.

In this model, the photon-nuclear density remains localized around $q = 0$ and $R = 2\ a_0$. The dynamics does not manifest any peculiar behavior along the R direction, since the wavepacket is transferred from S_1 to S_0 and back without major geometrical modification in the nuclear direction. Nonetheless, the dynamics along q is quite interesting: the cavity switches from the zero photon state to the one photon state, and back, thus, the density along q needs to evolve from the ground state to the first excited state, and back, of the harmonic oscillator. This is exactly what we observe in the evolution of the photon-nuclear density, shown as black contour lines in Fig. 9 at times $t = 0, 270, 540, 810$ a.t.u., that are, respectively, the initial time, one-quarter, half and three-quarters of the oscillation period of the average photon number.

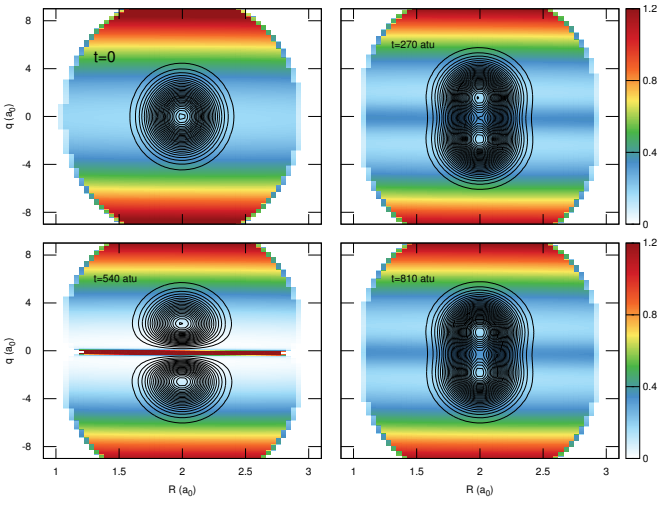

FIG. 9. Same as in Fig. 3 but for model *B*, at times $t = 0, 270, 540, 810$ a.t.u.

In order to produce the expected density in the q direction, the TDPES develops a very localized high barrier at $q = 0$ for all values of R. Upon closer inspection of the components of the TDPES (not reported), the main contribution to this barrier is ε_{geo}. Thus, once again we observe that the dynamics of the

TDPES along q is strongly dominated by this term, which is completely neglected in CTMQC. This observation explains the disagreement between CTMQC (in blue in Fig. 8) and QD results in describing the dynamics of the average photon number and of the S_1 population. MTE and TSH do not perform better than CTMQC, actually TSH provides once again a poorer description of the dynamics than MTE and CTMQC.

In the detailed analysis performed on model A, we observed in Fig. 4 that even though the major contribution to the potential barrier forming at $q = 0$ comes from $\varepsilon_{geo}(q,R,t)$, also $\varepsilon_{V_{PEN}}(q,R,t)$ presents a barrier. Indeed, such a smaller barrier has some effect on the marginal photon density reconstructed from the distribution of CTMQC trajectories in comparison to MTE and TSH. In Fig. 10, we report at times $t = 0, 270, 540$ a.t.u. the histograms calculated from the distributions of trajectories aiming to reproduce the marginal density along q with CTMQC (in blue, top panels), MTE (in red, middle panels) and TSH (in orange, bottom panels); the histograms are compared to the QD photonic marginal densities (black lines). All trajectory-based methods fail in reproducing the correct splitting of the density, thus underestimating the photon-emission process, even though at the final time reported in the figure, CTMQC shows the lowest presence of trajectories at $q = 0$, probably due to the presence of the small barrier in $\varepsilon_{V_{PEN}}(q,R,t)$. Such an effect is not, however, sufficient for producing a complete splitting of the density.

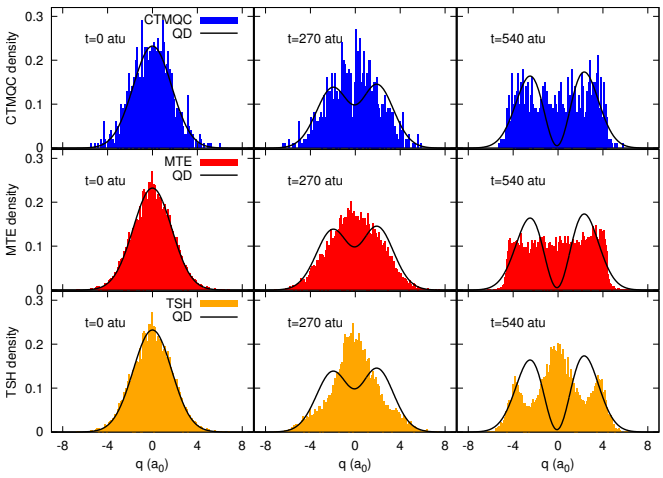

FIG. 10. Same as Fig. 7 but for model B, at times $t = 0, 270, 540$ a.t.u.

IV. DISCUSSION AND PERSPECTIVES

In the previous sections, we have developed the EF formalism to describe the dynamics of a PEN wavefunction with illustrative examples on model systems representing typical situations of nonadiabatic dynamics and spontaneous emission in the strong light-matter coupling regime as achievable in an optical cavity. Building upon previous work of Maitra and coworkers, we have proposed to treat the photonic and the nuclear degrees of freedom on equal footing, i.e., using the marginal amplitude in EF, with their dynamics taking place

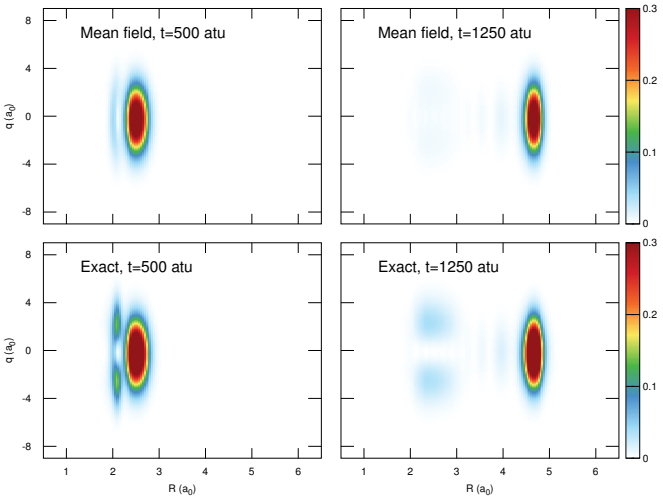

FIG. 11. Comparison of the mean-field photon-nuclear density (upper panels) with the exact density (lower panels) at times $t =$ 500 a.t.u. and $t = 1250$ a.t.u. for model A.

under the effect of the TDPES and the TDVP that account for the dynamics of the electrons. Applying this formulation of EF to CTMQC, we have treated the photon-nuclear dynamics using coupled trajectories. The comparison between the results of CTMQC simulations with QD simulations combined with the analysis of TDPES and TDVP allowed us to point out the key approximations done in CTMQC that lose validity when extended to treat "light" particles, as the photons in this case. Specifically, the geometric contribution of the TDPES becomes dominant in determining the shape of the TDPES, while it is completely neglected in the current formulation of CTMQC based on arguments depending on the small electron-nuclear mass ratio applied to the electron-nuclear formulation of EF[96]. Note that these observations are not limited to the case of PEN systems, but can be extended to other multi-component systems where EF and CTMQC are used, such as systems of protons and heavier nuclei or purely electronic systems. The question now arises as to whether including the geometric part of the TDPES for the photon-nuclear dynamics based on trajectories is sufficient to recover satisfactory performance of CTMQC or the corresponding contribution in the PENCO operator (17) in the electronic evolution equation is also need. Further studies are, however, needed to address this issue. Nonetheless, the numerical applications have shown an overall superior performance of CTMQC in comparison to MTE and TSH when applied to the examples proposed in Section III, even though we are well aware that these are simple model studies and that additional investigations are needed to generalize this observation.

In addition, we believe the classical treatment of photons within trajectory-based methods, as adopted in this work, emerges as a compelling alternative for advancing methodologies in the study of organic exciton polaritons[73,97]. Indeed, considering the significant number of electronic states inherent in organic excitons, the incorporation of the coupling between electronic and photonic degrees of freedom would re-

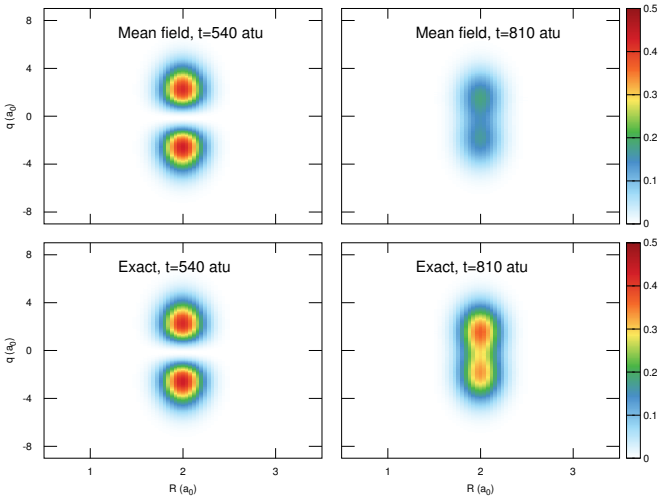

FIG. 12. Same as in Fig. 11 but for model B, at times $t = 540$ a.t.u. and $t = 810$ a.t.u.

sult in a substantial number of polaritonic states, potentially rendering the system unmanageable.

An interesting idea that we are in the process of exploring, and it is, thus, not developed here, is that of a "nested exact factorization". In this case, we would consider the marginal photon-nuclear amplitude $\chi(\boldsymbol{q},\boldsymbol{R},t)$ and the corresponding TDSE as the starting point of a new EF, which would lead to introduce, for instance, a marginal nuclear amplitude and a conditional photonic amplitude. The new evolution equations derived in this way, still under the effect of the TDPES and the TDVP, could potentially lead to develop more appropriate approximations for the photon dynamics. While, as mentioned above, this avenue is still to be fully investigated, the simplest approximation to such a photon-nuclear EF is an uncorrelated Hartree product[98] of the marginal photonic $\eta(\boldsymbol{q},t)$ and of the marginal nuclear $\zeta(\boldsymbol{R},t)$ wavefunction, namely

$$\chi(\boldsymbol{q},\boldsymbol{R},t) \simeq \chi^{mf}(\boldsymbol{q},\boldsymbol{R},t) = \zeta(\boldsymbol{R},t)\eta(\boldsymbol{q},t) \tag{30}$$

where the superscript mf stands for "mean-field". The performance of this approximation can be easily evaluated here using model A and model B. Specifically, based on QD results, we can define the mean-field photon-nuclear density as

$$|\chi^{mf}(\boldsymbol{q},\boldsymbol{R},t)|^2 = |\zeta(\boldsymbol{R},t)|^2|\eta(\boldsymbol{q},t)|^2 \tag{31}$$

where the marginal nuclear density is $|\zeta(\boldsymbol{R},t)|^2 = \int d\boldsymbol{q}|\chi(\boldsymbol{q},\boldsymbol{R},t)|^2$ and the marginal photonic density is $|\eta(\boldsymbol{q},t)|^2 = \int d\boldsymbol{R}|\chi(\boldsymbol{q},\boldsymbol{R},t)|^2$.

In Figs. 11 and 12, we compare the exact photon-nuclear density (lower panels) at times $t = 500$ a.t.u. and $t = 1250$ a.t.u. for model A and at times $t = 540$ a.t.u. and $t = 810$ a.t.u. for model B, respectively, with their corresponding mean-field approximations (upper panels). Note that this analysis is different from the work by Maitra and coworkers[38], where the performance of the mean-field approximation in terms of MTE was investigated between the photons and the electrons. Here, we aim to retain the full correlation between the electronic and the photon-nuclear dynamics, while investigating the effect of the mean-field treatment of the photonic and nuclear coupling for the particular dynamics studied in this work. Indeed, we note that, as expected, the details of the dynamics are slightly washed out, but the mean-field approximation seems to perform quite well. The mean-field approximation analyzed in Figs. 11 and 12 via Eq. (31) is to be considered the "best" possible mean-field description of the photon-nuclear density since it is derived using the exact QD density as starting point to define the marginal densities.

The interesting property of the uncorrelated Hartree product is that, when inserted into Eq. (9), it yields straightforwardly evolution equations for the marginal amplitudes in the form of TDSEs, where the effects of the TDPES and of the TDVP is averaged over the marginal amplitudes themselves. Namely, inserting the Hartree product form given in Eq. (30) into Eq. (9), we can derive the evolution equations for the marginal amplitudes, by multiplying by $\eta^*(\boldsymbol{q},t)$ and integrating over $\boldsymbol{q}$ or by multiplying by $\chi^*(\boldsymbol{R},t)$ and integrating over $\boldsymbol{R}$, thus obtaining

$$i\frac{\partial\zeta(\boldsymbol{R},t)}{\partial t} = \left[\sum_\alpha \frac{\left(-i\nabla_\alpha + \langle \mathbf{A}_\alpha(\boldsymbol{q},\boldsymbol{R},t)\rangle_\eta\right)^2}{2M_\alpha} + \hat{V}^P_{mf}(\boldsymbol{R},t)\right]\zeta(\boldsymbol{R},t) \tag{32}$$

$$i\frac{\partial\eta(\boldsymbol{q},t)}{\partial t} = \left[\sum_\nu \frac{\left(-i\nabla_\nu + \langle \mathbf{S}_\nu(\boldsymbol{q},\boldsymbol{R},t)\rangle_\zeta\right)^2}{2} + \hat{V}^N_{mf}(\boldsymbol{q},t)\right]\eta(\boldsymbol{q},t) \tag{33}$$

Here, we have defined the "weighted" $\boldsymbol{R}$-TDVP over the photonic wavefunction, i.e., $\langle \mathbf{A}_\alpha(\boldsymbol{q},\boldsymbol{R},t)\rangle_\eta = \langle\eta(\boldsymbol{q},t)|\mathbf{A}_\alpha(\boldsymbol{q},\boldsymbol{R},t)|\eta(\boldsymbol{q},t)\rangle_{\boldsymbol{q}}$, where the the symbol $\langle\cdot\rangle_{\boldsymbol{q}}$ indicates an integration over $\boldsymbol{q}$, and the

"weighted" $\boldsymbol{q}$-TDVP over the nuclear wavefunction, i.e., $\langle \mathbf{S}_\nu(\boldsymbol{q},\boldsymbol{R},t)\rangle_\zeta = \langle \zeta(\boldsymbol{R},t)|\mathbf{S}_\nu(\boldsymbol{q},\boldsymbol{R},t)|\zeta(\boldsymbol{R},t)\rangle_{\boldsymbol{R}}$, where the the symbol $\langle\cdot\rangle_{\boldsymbol{R}}$ stands for an integration over nuclear positions. In addition, the effect of the photons in Eq. (32) is encoded in the photonic mean-field potential $\hat{V}^P_{mf}(\boldsymbol{R},t)$,

$$\hat{V}^P_{mf}(\boldsymbol{R},t) = \left\langle \eta(\boldsymbol{q},t)\left|\sum_\nu \hat{\tilde{T}}_\nu + \varepsilon(\boldsymbol{q},\boldsymbol{R},t) - i\partial_t\right|\eta(\boldsymbol{q},t)\right\rangle_{\boldsymbol{q}} \tag{34}$$

where $\hat{\tilde{T}}_\nu = \frac{1}{2}(-i\nabla_\nu + \mathbf{S}_\nu(\boldsymbol{q},\boldsymbol{R},t))^2$ expresses the kinetic contribution of the photons averaged over the photonic wavefunction. Similarly, the effect of the nuclei in Eq. (33) is encoded in the nuclear mean-field potential $\hat{V}^N_{mf}(\boldsymbol{q},t)$, namely

$$\hat{V}^N_{mf}(\boldsymbol{q},t) = \left\langle \zeta(\boldsymbol{R},t)\left|\sum_\alpha \hat{\tilde{T}}_\alpha + \varepsilon(\boldsymbol{q},\boldsymbol{R},t) - i\partial_t\right|\zeta(\boldsymbol{R},t)\right\rangle_{\boldsymbol{R}} \tag{35}$$

with $\hat{\tilde{T}}_\alpha = \frac{1}{2M_\alpha}(-i\nabla_\alpha + \mathbf{A}_\alpha(\boldsymbol{q},\boldsymbol{R},t))^2$ the kinetic contribution of the nuclei averaged over the nuclear wavefunction.

Furthermore, expressing the nuclear wavefunction $\zeta(\boldsymbol{R},t)$ and the photonic wavefunction $\eta(\boldsymbol{q},t)$ in polar forms enables us to derive the equations governing the evolution of their phases, $W_N(\boldsymbol{R},t)$ and $W_P(\boldsymbol{q},t)$, respectively. Interestingly, similarly to the EF of the electron-nuclear wavefunction, these equations have the form of Hamilton-Jacobi equations, namely

$$-\frac{\partial W_N}{\partial t} = \sum_\alpha \frac{(\nabla_\alpha W_N + \langle \mathbf{A}_\alpha(\boldsymbol{q},\boldsymbol{R},t)\rangle_\eta)^2}{2M_\alpha} + \hat{V}^P_{mf}(\boldsymbol{R},t) + \mathscr{Q}^{mf}_{\boldsymbol{R}}(\boldsymbol{R},t) + \sigma(\langle \mathbf{A}_\alpha(\boldsymbol{q},\boldsymbol{R},t)\rangle_\eta) \tag{36}$$

$$-\frac{\partial W_P}{\partial t} = \sum_{\nu=1}^{N_P} \frac{(\nabla_\nu W_P + \langle \mathbf{S}_\nu(\boldsymbol{q},\boldsymbol{R},t)\rangle_\zeta)^2}{2} + \hat{V}^N_{mf}(\boldsymbol{q},t) + \mathscr{Q}^{mf}_{\boldsymbol{q}}(\boldsymbol{q},t) + \sigma(\langle \mathbf{S}_\nu(\boldsymbol{q},\boldsymbol{R},t)\rangle_\zeta) \tag{37}$$

and are potentially solvable using the method of characteristics, as it has been illustrated in detailed for the derivation of CTMQC[93]. Note, however, that apart from the "standard" quantum potentials $\mathscr{Q}^{mf}_{\boldsymbol{R}}(\boldsymbol{R},t) = -\frac{1}{2M_\alpha}\frac{\nabla^2|\zeta(\boldsymbol{R},t)|}{|\zeta(\boldsymbol{R},t)|}$ and $\mathscr{Q}^{mf}_{\boldsymbol{q}}(\boldsymbol{q},t) = -\frac{1}{2}\frac{\nabla^2|\eta(\boldsymbol{q},t)|}{|\eta(\boldsymbol{q},t)|}$, which are usually neglected within a classical-like treatment of the dynamics, additional (and new) effects appear via $\sigma(\langle \mathbf{A}_\alpha(\boldsymbol{q},\boldsymbol{R},t)\rangle_\eta) = \sum_\alpha \frac{\langle \mathbf{A}^2_\alpha(\boldsymbol{q},\boldsymbol{R},t)\rangle_\eta - \langle \mathbf{A}_\alpha(\boldsymbol{q},\boldsymbol{R},t)\rangle^2_\eta}{2M_\alpha}$ and $\sigma(\langle \mathbf{S}_\nu(\boldsymbol{q},\boldsymbol{R},t)\rangle_\zeta) = \sum_\nu \frac{\langle \mathbf{S}^2_\nu(\boldsymbol{q},\boldsymbol{R},t)\rangle_\zeta - \langle \mathbf{S}_\nu(\boldsymbol{q},\boldsymbol{R},t)\rangle^2_\zeta}{2}$ that look like standard deviations of the weighted TDVPs.

The ideas developed in this work and the additional investigation avenues briefly sketched in this section show that the EF formalism offers a rich range of possibilities to analyze the dynamics of multi-component systems under different perspectives and to propose algorithms for molecular-dynamics simulations based on trajectories. The implications of these approximations can only be assessed through numerical tests, and this constitutes a subject for future study.

V. CONCLUSIONS

In this work, the formalism of the exact factorization was extended to treat the photon-electron-nuclear dynamics, to describe the coupled motion of photons, electrons, and nuclei at the quantum-mechanical level. The factorization choice was the one where the marginal amplitude is chosen as the wavefunction for the photon-nuclear subsystem, and the electronic subsystem is then conditionally dependent on the photon-nuclear positions. This choice is particularly interesting since, when CTMQC is employed for trajectory-based simulations, it suggests a treatment of photonic and nuclear degrees of freedom on equal footing in terms of coupled trajectories. In this way, the full correlation with the electronic subsystem is maintained, clearly within the approximations underlying CTMQC.

Aiming to assess the quality of CTMQC dynamics for photon-electron-nuclear problems, we have studied two model situations illustrating nonadiabatic dynamics and spontaneous emission of an electron-nuclear system strongly coupled to a single-mode cavity in resonance with a typical electronic excitation window of the system. Our analysis of the exact factorization formalism was based on the analysis of the time-dependent potentials of the theory combined with the assessment of the performance of CTMQC. In particular, we employed the results of numerically-exact quantum-dynamics simulations as benchmark for CTMQC and we compared CTMQC with multi-trajectory Ehrenfest and with Tully surface hopping. The calculations revealed that CTMQC and Ehrenfest presented better agreement with exact quantum dynamics than surface hopping in terms of average photon numbers and electronic populations all along the dynamics. How-

ever, quantitative agreement with the reference results is lacking across all methods, but we pointed out the most probable source of error in CTMQC, which will be investigated further in the future. Specifically, the geometric component the time-dependent potential energy surface, which is neglected in CTMQC, showed to be dominant along the photonic coordinate for the considered systems, as it seems to have significant effect in the splitting of the photon density.

The implications of the photon-nuclear correlation were investigated by comparing the exact photon-nuclear density and the uncorrelated Hartree product for both models considered, while keeping intact the correlation with electronic subsystem. In general, as expected, such a mean-field approximation washes out some details of the dynamics. However, the equations for the marginal photonic and nuclear amplitudes seem interesting, especially in view of their possible solution in terms of trajectories.

ACKNOWLEDGEMENTS

This work was supported by a public grant from the Laboratoire d'Excellence Physics Atoms Light Matter (LabEx PALM) overseen by the French National Research Agency (ANR) as part of the "Investissements d'Avenir" program (reference: ANR-10-LABX-0039-PALM), by the ANR Q-DeLight project, Grant No. ANR-20-CE29-0014 of the French Agence Nationale de la Recherche.

[1] A. Abedi, N. T. Maitra, and E. K. U. Gross, "Exact factorization of the time-dependent electron-nuclear wave function," Phys. Rev. Lett. **105**, 123002 (2010).
[2] A. Abedi, N. T. Maitra, and E. K. U. Gross, "Correlated electron-nuclear dynamics: Exact factorization of the molecular wavefunction," J. Chem. Phys. **137**, 22A530 (2012).
[3] F. Agostini and E. K. Gross, "Ultrafast dynamics with the exact factorization," Eur. Phys. J. B **94** (2021), 10.1140/epjb/s10051-021-00171-2.
[4] L. M. Ibele, C. Pieroni, F. Talotta, B. F. Curchod, D. Lauvergnat, and F. Agostini, "Exact factorization of the electron-nuclear wavefunction: Fundamentals and algorithms," in *Comprehensive Computational Chemistry, Russell Boyd and Manuel Yanez* (Elsevier, 2023).
[5] F. Agostini, A. Abedi, Y. Suzuki, S. K. Min, N. T. Maitra, and E. K. U. Gross, "The exact forces on classical nuclei in non-adiabatic charge transfer," J. Chem. Phys. **142**, 084303 (2015).
[6] B. F. E. Curchod and F. Agostini, "On the dynamics through a conical intersection," J. Phys. Chem. Lett. **8**, 831–837 (2017).
[7] L. M. Ibele, B. F. E. Curchod, and F. Agostini, "A photochemical reaction in different theoretical representations," J. Phys. Chem. A **126**, 1263–1281 (2022).
[8] L. M. Ibele, E. Sangiogo Gil, B. F. E. Curchod, and F. Agostini, "On the nature of geometric and topological phases in the presence of conical intersections," J. Phys. Chem. Lett. **14**, 11625–11631 (2023).
[9] S. K. Min, F. Agostini, and E. K. U. Gross, "Coupled-trajectory quantum-classical approach to electronic decoherence in nonadiabatic processes," Phys. Rev. Lett. **115**, 073001 (2015).
[10] F. Agostini, S. K. Min, A. Abedi, and E. K. U. Gross, "Quantum-classical nonadiabatic dynamics: Coupled- vs independent-trajectory methods," J. Chem. Theory Comput. **12**, 2127–2143 (2016).
[11] S. K. Min, F. Agostini, I. Tavernelli, and E. K. U. Gross, "Ab initio nonadiabatic dynamics with coupled trajectories: A rigorous approach to quantum (de)coherence," J. Phys. Chem. Lett. **8**, 3048–3055 (2017).
[12] J.-K. Ha, I. S. Lee, and S. K. Min, "Surface hopping dynamics beyond nonadiabatic couplings for quantum coherence," J. Phys. Chem. Lett. **9**, 1097–1104 (2018).
[13] G. H. Gossel, F. Agostini, and N. T. Maitra, "Coupled-trajectory mixed quantum-classical algorithm: A deconstruction," J. Chem. Theory Comput. **14**, 4513–4529 (2018).
[14] F. Agostini, "An exact-factorization perspective on quantum-classical approaches to excited-state dynamics," Eur. Phys. J. B **91** (2018).
[15] F. Talotta, F. Agostini, and G. Ciccotti, "Quantum trajectories for the dynamics in the exact factorization framework: a proof-of-principle test," J. Phys. Chem. A **124**, 6764–6777 (2020).
[16] F. Talotta, S. Morisset, N. Rougeau, D. Lauvergnat, and F. Agostini, "Spin-orbit interactions in ultrafast molecular processes," Phys. Rev. Lett. **124**, 033001 (2020).
[17] M. Schirò, F. G. Eich, and F. Agostini, "Quantum-classical nonadiabatic dynamics of Floquet driven systems," J. Chem. Phys. **154**, 114101 (2021).
[18] C. Pieroni and F. Agostini, "Nonadiabatic dynamics with coupled trajectories," J. Chem. Theory Comput. **17**, 5969–5991 (2021).
[19] J.-K. Ha and S. K. Min, "Independent trajectory mixed quantum-classical approaches based on the exact factorization," J. Chem. Phys. **156**, 174109 (2022).
[20] D. Han, J.-K. Ha, and S. K. Min, "Real-space and real-time propagation for correlated electron-nuclear dynamics based on exact factorization," J. Chem. Theory Comput. **19**, 2186–2197 (2023).
[21] E. V. Arribas, L. M. Ibele, D. Lauvergnat, N. T. Maitra, and F. Agostini, "Significance of energy conservation in coupled-trajectory approaches to nonadiabatic dynamics," J. Chem Theory Comput. **19**, 7787–7800 (2023).
[22] A. Dines, M. Ellis, and J. Blumberger, "Stabilized coupled trajectory mixed quantum-classical algorithm with improved energy conservation: CTMQC-EDI," J. Chem. Phys. **159**, 234118 (2023).
[23] E. Villaseco Arribas and N. T. Maitra, "Energy-conserving coupled trajectory mixed quantum-classical dynamics," J. Chem. Phys. **158** (2023).
[24] C. Pieroni, E. Sangiogo Gil, L. M. Ibele, M. Persico, G. Granucci, and F. Agostini, "Investigating the photodynamics of trans-azobenzene with coupled trajectories," J. Chem. Theory Comput **20**, 580–596 (2024).
[25] D. Han and A. Akimov, "Nonadiabatic dynamics with exact factorization: Implementation and assessment," J. Chem. Theory Comput. , doi: 10.1021/acs.jctc.4c00343 (2024).
[26] M. Born and R. Oppenheimer, "Zur Quantentheorie der Molekeln," Ann. Phys. **84**, 457–484 (1927).
[27] F. Agostini and B. F. E. Curchod, "When the exact factorization meets conical intersections..." Eur. Phys. J. B **91**, 141 (2018).
[28] A. Schild and E. K. U. Gross, "Exact single-electron approach to the dynamics of molecules in strong laser fields," Phys. Rev. Lett. **118**, 163202 (2017).
[29] J. Koć́k, E. Kraisler, and A. Schild, "Charge-transfer steps in density functional theory from the perspective of the exact electron factorization," J. Phys. Chem. Lett. **12**, 3204–3209 (2021).
[30] J. Kocák and A. Schild, "Many-electron effects of strong-field ionization described in an exact one-electron theory," Phys. Rev. Research **2**, 043365 (2020).
[31] L. Lacombe and N. T. Maitra, "Embedding via the exact factorization approach," Phys. Rev. Lett. **124**, 206401 (2020).
[32] E. K. U. G. Ryan Requist, "Fock space embedding theory for strongly correlated topological phases," Phys. Rev. Lett. **127**, 116401 (2019).
[33] S. Giarrusso, P. Gori-Giorgi, and F. Agostini, "Electronic vector potential from the exact factorization of a complex wavefunction," ChemPhysChem **n/a**, e202400127 (2024).
[34] N. M. Hoffmann, H. Appel, A. Rubio, and N. T. Maitra, "Light-matter interactions via the exact factorization approach," Eur. Phys. J. B **91**, 180 (2018).
[35] A. Abedi, E. Khosravi, and I. V. Tokatly, "Shedding light on correlated electron–photon states using the exact factorization," Eur. Phys. J. B **91**, 194 (2018).
[36] L. Lacombe, N. M. Hoffmann, and N. T. Maitra, "Exact potential energy surface for molecules in cavities," Phys. Rev. Lett. **123**, 083201 (2019).
[37] P. Martinez, B. Rosenzweig, N. M. Hoffmann, L. Lacombe, and N. T. Maitra, "Case studies of the time-dependent potential energy surface for dynamics in cavities," J. Chem. Phys. **154**, 014102 (2021).
[38] B. Rosenzweig, N. M. Hoffmann, L. Lacombe, and N. T. Maitra, "Analysis of the classical trajectory treatment of photon dynamics for polaritonic phenomena," J. Chem. Phys. **156**, 054101 (2022).

[39]J. A. Hutchison, T. Schwartz, C. Genet, E. Devaux, and T. W. Ebbesen, "Modifying chemical landscapes by coupling to vacuum fields," Angew. Chem. Int. Ed. **51**, 1592 (2012).
[40]S. Wang, T. Chervy, J. George, J. A. Hutchison, C. Genet, and T. W. Ebbesen, "Quantum yield of polariton emission from hybrid light-matter states," J. Phys. Chem. Lett. **5**, 1433 (2014).
[41]T. W. Ebbesen, "Hybrid light-matter states in a molecular and material science perspective," Acc. Chem. Res. **49**, 2403 (2016).
[42]L. A. Martínez-Martínez, M. Du, R. F. Ribeiro, S. Kéa-Cohen, and J. Yuen-Zhou, "Polariton-assisted singlet fission in acene aggregates," J. Phys. Chem. Lett. **9**, 1951 (2018).
[43]M. Du, L. A. Martínez-Martínez, R. F. Ribeiro, Z. Hu, V. M. Menon, and J. Yuen-Zhou, "Theory for polariton-assisted remote energy transfer," Chem. Sci. **9**, 6659 (2018).
[44]L. A. Martínez-Martínez, R. F. Ribeiro, J. Campos-González-Angulo, and J. Yuen-Zhou, "Can ultrastrong coupling change ground-state chemical reactions?" ACS Photonics **5**, 167 (2018).
[45]R. T. Grant, P. Michetti, A. J. Musser, P. Gregoire, T. Virgili, E. Vella, M. Cavazzini, K. Georgiou, F. Galeotti, C. Clark, J. Clark, C. Silva, and D. G. Lidzey, "Efficient radiative pumping of polaritons in a strongly coupled microcavity by a fluorescent molecular dye," Adv. Optical Mater. **4**, 1615 (2016).
[46]V. C. Nikolis, A. Mischok, B. Siegmund, J. Kublitski, X. Jia, J. Benduhn, U. Hörmann, D. Neher, M. C. Gather, D. Spoltore, and K. Vandewal, "Strong light-matter coupling for reduced photon energy losses in organic photovoltaics," Nat. Comm. **10**, 3706 (2019).
[47]P. Vasa and C. Lienau, "Strong light-matter interaction in quantum emitter/metal hybrid nanostructures," ACS Photonics **5**, 2 (2018).
[48]D. G. Baranov, M. Wersäll, J. Cuadra, T. J. Antosiewicz, and T. Shegai, "Novel nanostructures and materials for strong light-matter interactions," ACS Photonics **5**, 24 (2018).
[49]J. T. Hugall, A. Singh, and N. F. van Hulst, "Plasmonic cavity coupling," ACS Photonics **5**, 43 (2018).
[50]E. Orgiu, J. George, J. A. Hutchison, E. Devaux, J. F. Dayen, B. Doudin, F. Stellacci, C. Genet, J. Schachenmayer, C. Genes, G. Pupillo, P. Samori, , and T. W. Ebbesen, "Conductivity in organic semiconductors hybridized with the vacuum field," Nat. Mater. **14**, 1123 (2015).
[51]J. Feist, J. Galego, and F. J. Garcia-Vidal, "Polaritonic chemistry with organic molecules," ACS Photonics **5**, 205–216 (2018).
[52]J. Fregoni, F. J. Garcia-Vidal, and J. Feist, "Theoretical challenges in polaritonic chemistry," ACS Photonics **9**, 1096–1107 (2022).
[53]J. Galego, F. J. Garcia-Vidal, and J. Feist, "Cavity-induced modifications of molecular structure in the strong-coupling regime," Phys. Rev. X **5**, 041022 (2015).
[54]J. Galego and F. J. G.-V. J. Feist, "Many-molecule reaction triggered by a single photon in polaritonic chemistry," Phys. Rev. Lett. **119**, 136001 (2017).
[55]T. E. Li, A. Nitzan, and J. E. Subotnik, "Cavity molecular dynamics simulations of vibrational polariton-enhanced molecular nonlinear absorption," J. Chem. Phys. **154**, 094124 (2021).
[56]T. E. Li, A. Nitzan, and J. E. Subotnik, "Polariton relaxation under vibrational strong coupling: Comparing cavity molecular dynamics simulations against Fermi?s golden rule rate," J. Chem. Phys. **156**, 134106 (2022).
[57]M. R. Fiechter, J. E. Runeson, J. E. Lawrence, and J. O. Richardson, "How quantum is the resonance behavior in vibrational polariton chemistry?" J. Phys. Chem. Lett. **14**, 8261–8267 (2023).
[58]Y. Ke and J. Richardson, "Quantum nature of reactivity modification in vibrational polariton chemistry," ChemRxiv (2024), 10.26434/chemrxiv-2024-nfmpk.
[59]E. Hulkko, S. Pikker, V. Tiainen, R. H. Tichauer, G. Groenhof, and J. J. Toppari, "Effect of molecular stokes shift on polariton dynamics," J. Chem. Phys. **154**, 154303 (2021).
[60]R. H. Tichauer, J. Feist, and G. Groenhof, "Multi-scale dynamics simulations of molecular polaritons: The effect of multiple cavity modes on polariton relaxation," J. Chem. Phys. **154**, 104112 (2021).
[61]R. H. Tichauer, D. Morozov, I. Sokolovskii, J. J. Toppari, and G. Groenhof, "Identifying vibrations that control non-adiabatic relaxation of polaritons in strongly coupled molecule?cavity systems," J. Phys. Chem. Lett. **13**, 6259–6267 (2022).
[62]J. Flick, H. Appel, M. Ruggenthaler, and A. Rubio, "Cavity Born-Oppenheimer approximation for correlated electron-nuclear-photon systems," J. Chem. Theory Comput. **13**, 1616–1625 (2017).
[63]M. R. Fiechter and J. O. Richardson, "Understanding the cavity Born?Oppenheimer approximation," J. Chem. Phys. **160**, 184107 (2024).
[64]E. W. Fischer and P. Saalfrank, "Beyond cavity Born-Oppenheimer: On nonadiabatic coupling and effective ground state hamiltonians in vibropolaritonic chemistry," J. Chem. Theory Comput. **19**, 72157229 (2023).
[65]A. Z. Lieberherr, S. T. E. Furniss, J. E. Lawrence, and D. E. Manolopoulos, "Vibrational strong coupling in liquid water from cavity molecular dynamics," J. Chem. Phys. **158**, 234106 (2023).
[66]M. Kowalewski, K. Bennett, and S. Mukamel, "Cavity femtochemistry: Manipulating nonadiabatic dynamics at avoided crossings," J. Phys. Chem. Lett. **7**, 2050 (2016).
[67]B. Gu and S. Mukamel, "Optical-cavity manipulation of conical intersections and singlet fission dynamics," in *Frontiers in Optics + Laser Science 2021* (Optica Publishing Group, 2021) p. LTh2E.1.
[68]B. Rana, E. G. Hohenstein, and T. J. Martínez, "Simulating the excited-state dynamics of polaritons with ab initio multiple spawning," J. Phys. Chem. A **128**, 139–151 (2024).
[69]H.-T. Chen, T. E. Li, M. Sukharev, A. Nitzan, and J. E. Subotnik, "Ehrenfest+R dynamics. I. A mixed quantum?classical electrodynamics simulation of spontaneous emission," J. Chem. Phys. **150**, 044102 (2019).
[70]T. E. Lia, J. E. Subotnik, and A. Nitzan, "Cavity molecular dynamics simulations of liquid waterunder vibrational ultrastrong coupling," Proc. Natl. Acad. Sci. U.S.A. **117**, 18324–18331 (2020).
[71]T. E. Li, A. Nitzan, and J. E. Subotnik, "Collective vibrational strong coupling effects on molecular vibrational relaxation and energy transfer: Numerical insights via cavity molecular dynamics simulations," Ang. Chemie Int. Ed. **60**, 15533–15540 (2021).
[72]T. E. Li, B. Cui, J. E. Subotnik, and A. Nitzan, "Molecular polaritonics: Chemical dynamics under strong light?matter coupling," Annu. Rev. Phys. Chem. **73**, 43–71 (2022).
[73]H. L. Luk, J. Feist, J. J. Toppari, and G. Groenhof, "Multiscale molecular dynamics simulations of polaritonic chemistry," J. Chem. Theory Comput. **13**, 4324–4335 (2017).
[74]J. Fregoni, G. Granucci, E. Coccia, M. Persico, and S. Corni, "Manipulating azobenzene photoisomerization through strong light-molecule coupling," Nat. Commun **9**, 4688 (2018).
[75]J. Fregoni, S. Corni, M. Persico, and G. Granucci, "Photochemistry in the strong coupling regime: A trajectory surface hopping scheme," J. Chem. Phys. **41**, 2033–2044 (2020).
[76]J. Fregoni, G. Granucci, M. Persico, and S. Corni, "Strong coupling with light enhances the photoisomerization quantum yield of azobenzene," Chem **6**, 250–265 (2020).
[77]N. M. Hoffmann, C. Schäfer, A. Rubio, A. Kelly, and H. Appel, "Capturing vacuum fluctuations and photon correlations in cavity quantum electrodynamics with multitrajectory Ehrenfest dynamics," Phys. Rev. A **99**, 063819 (2019).
[78]O. Vendrell, "Collective Jahn-Teller interactions through light-matter coupling in a cavity," Phys. Rev. Lett. **121**, 253001 (2018).
[79]B. Rana, E. G. Hohenstein, and T. J. Martínez, "Simulating the excited-state dynamics of polaritons with ab initio multiple spawning," J. Phys. Chem. A **128**, 139–151 (2023).
[80]J. Flick, M. Ruggenthaler, H. Appel, and A. Rubio, "Kohn-Sham approach to quantum electrodynamical density-functional theory: Exact time-dependent effective potentials in real space," Proc. Natl. Acad. Sci. U.S.A. **112**, 15285 (2015).
[81]J. Flick, D. M. Welakuh, M. Ruggenthaler, H. Appel, and A. Rubio, "Light-matter response in nonrelativistic quantum electrodynamics," ACS Photonics **6**, 2757–2778 (2019).
[82]C. Schäfer, M. Ruggenthaler, H. Appel, and A. Rubio, "Modification of excitation and charge transfer in cavity quantum-electrodynamical chemistry," Proc. Natl. Acad. Sci. U.S.A. **116**, 4883 (2019).
[83]J. Yang, Q. Ou, Z. Pei, H. Wang, B. Weng, Z. Shuai, K. Mullen, and Y. Shao, "Quantum-electrodynamical time-dependent density functional theory within Gaussian atomic basis," The Journal of Chemical Physics **155**, 064107 (2021).
[84]U. Mordovina, C. Bungey, H. Appel, P. J. Knowles, A. Rubio, and F. R. Manby, "Polaritonic coupled-cluster theory," Phys. Rev. Research **2**,

023262 (2020).
[85]S. Angelico, T. S. Haugland, E. Ronca, and H. Koch, "Coupled cluster cavity Born-Oppenheimer approximation for electronic strong coupling," J. Chem. Phys. **159**, 214112 (2023).
[86]N. M. Hoffmann, L. Lacombe, A. Rubio, and N. T. Maitra, "Effect of many modes on self-polarization and photochemical suppression in cavities," J. Chem. Phys. **153**, 104103 (2020).
[87]E. A. Power, S. Zienau, and H. S. W. Massey, "Coulomb gauge in non-relativistic quantum electro-dynamics and the shape of spectral lines," Phil. Trans. R. Soc. A **251**, 427–454 (1959).
[88]E. W. Fischer and P. Saalfrank, "Beyond cavity born?oppenheimer: On nonadiabatic coupling and effective ground state hamiltonians in vibro-polaritonic chemistry," J. Chem. Theory Comput. **19**, 7215–7229 (2023).
[89]M. Ruggenthaler, J. Flick, C. Pellegrini, H. Appel, I. V. Tokatly, and A. Rubio, "Quantum-electrodynamical density-functional theory: Bridging quantum optics and electronic-structure theory," Phys. Rev. A **90**, 012508 (2014).
[90]M. Ruggenthaler, N. Tancogne-Dejean, J. Flick, H. Appel, and A. Rubio, "From a quantum-electrodynamical light?matter description to novel spectroscopies," Nat. Rev. Chem. **2**, 0118 (2018).
[91]F. Agostini and B. F. E. Curchod, "Chemistry without the Born-Oppenheimer approximation," Phil. Trans. R. Soc. A **380**, 20200375 (2022).
[92]F. Talotta, S. Morisset, N. Rougeau, D. Lauvergnat, and F. Agostini, "Internal conversion and intersystem crossing with the exact factorization," J. Chem Theory Comput. **16**, 4833–4848 (2020).
[93]F. Agostini, I. Tavernelli, and G. Ciccotti, "Nuclear quantum effects in electronic (non) adiabatic dynamics," Eur. Phys. J. B **91**, 1–12 (2018).
[94]D. Lauvergnat, "QuantumModelLib," (accessed in June 2024), `https://github.com/lauvergn/QuantumModelLib`.
[95]F. Agostini, E. Marsili, F. Talotta, C. Pieroni, E. Villaseco Arribas, L. M. Ibele, and E. Sangiogo Gil, "G-CTMQC," (accessed in June 2024), `https://gitlab.com/agostini.work/g-ctmqc`.
[96]F. G. Eich and F. Agostini, "The adiabatic limit of the exact factorization of the electron-nuclear wave function," J. Chem. Phys. **145**, 054110 (2016).
[97]I. Sokolovskii and G. Groenhof, "Photochemical initiation of polariton-mediated exciton propagation," Nanophotonics **13**, 2687–2694 (2024).
[98]F. Agostini, E. K. U. Gross, and B. F. E. Curchod, "Electron-nuclear entanglement in the time-dependent molecular wavefunction," Comput. Theo. Chem. **1151**, 99–106 (2019).